*International Tables for Crystallography* (2012). Vol. F, Chapter 8.1, pp. 189–204.

# PART 8. SYNCHROTRON CRYSTALLOGRAPHY

## Chapter 8.1. Synchrotron-radiation instrumentation, methods and scientific utilization

J. R. Helliwell

### 8.1.1. Introduction

Synchrotron radiation (SR) has had a profound impact on the field of protein crystallography. The properties of high spectral brightness and tunability have enabled higher-resolution structure determinations, multiple-wavelength anomalous-dispersion (MAD) techniques, studies of much larger molecular weight structures, the use of small crystals and dynamical time-resolved structural studies. The use of SR required development of suitable X-ray beamline optics for focusing and monochromatization of the beam, which had to be stable in position and spectral character, for rotating-crystal data collection. Finely focused polychromatic beams have been used for ultra-fast data collection with the most advanced SR sources, where a single bunch pulse of X-rays can be strong enough to yield Laue diffraction data. The optimal recording of the diffraction patterns has necessitated the development of improved area detectors, along with associated data-acquisition hardware and data-processing algorithms. Sample cooling and freezing have reduced and greatly diminished, although not eliminated, radiation damage, respectively. In turn, even smaller crystals have been used. However, new X-radiation damage challenges are being reached. The low emittance of SR sources, with their small source size and beam divergence, corresponds well with the small size and low mosaicity of protein crystal samples. The evolution of SR source spectral brightness each year over the last twenty years has changed by many orders of magnitude, a remarkable trend in technical capability.

### 8.1.2. The physics of SR

The physics of the SR source spectral emission was predicted by Iwanenko & Pomeranchuk (1944) and Blewett (1946), and was fully described by Schwinger (1949). It is 'universal' to all machines of this type, *i.e.*, wherever charged particles such as electrons (or positrons) travel in a curved orbit under the influence of a magnetic field, and are therefore subject to centripetal acceleration. At a speed very near the speed of light, the relativistic particle emission is concentrated into a tight, forward radiation cone angle. There is a continuum of Doppler-shifted frequencies from the orbital frequency up to a cutoff. The radiation is also essentially plane-polarized in the orbit plane. However, in high-energy physics machines, the beam used in target or colliding-beam experiments would be somewhat unstable; thus, while pioneering experiments ensued through the 1970s, a considerable appetite was stimulated for machines dedicated to SR with stable source position, for fine focusing onto small samples such as crystals and single fibres, and with a long beam lifetime for more challenging data collection. Crystallography has been both an instigator and major beneficiary of these developments through the 1970s and 1980s onwards. An example of a machine lattice (the ESRF) is shown in Fig. 8.1.2.1.

The properties of synchrotron radiation can be described in terms of the well defined quantities of high flux (a large number of photons), high angular brightness (also well collimated), high spectral brightness (also a small source size and well collimated), tunable, polarized, defined time structure (fine time resolution) and exactly calculable spectra. The precise definition of the spectral brightness is

$$\text{Spectral brightness} = \text{photons per s per mm}^2 \text{ per mrad}^2 \text{ per (0.1\% bandwidth).} \quad (8.1.2.1)$$

Care needs to be exercised to check precisely the definition in use (Mills *et al.*, 2005). The mrad$^2$ term refers to the radiation solid angle delivered from the source, and the mm$^2$ term to the source cross-sectional area. Mills *et al.* (2005) concluded that the units given in equation (8.1.2.1), which do not follow the SI code for

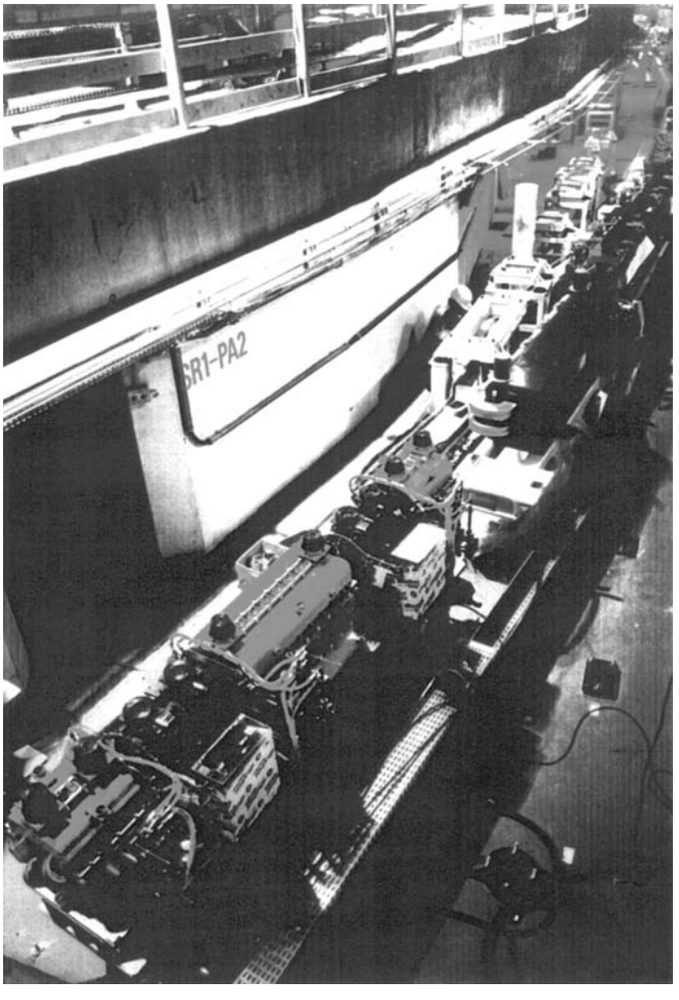


**Figure 8.1.2.1**
The ring tunnel and part of the machine lattice at the ESRF, Grenoble, France.

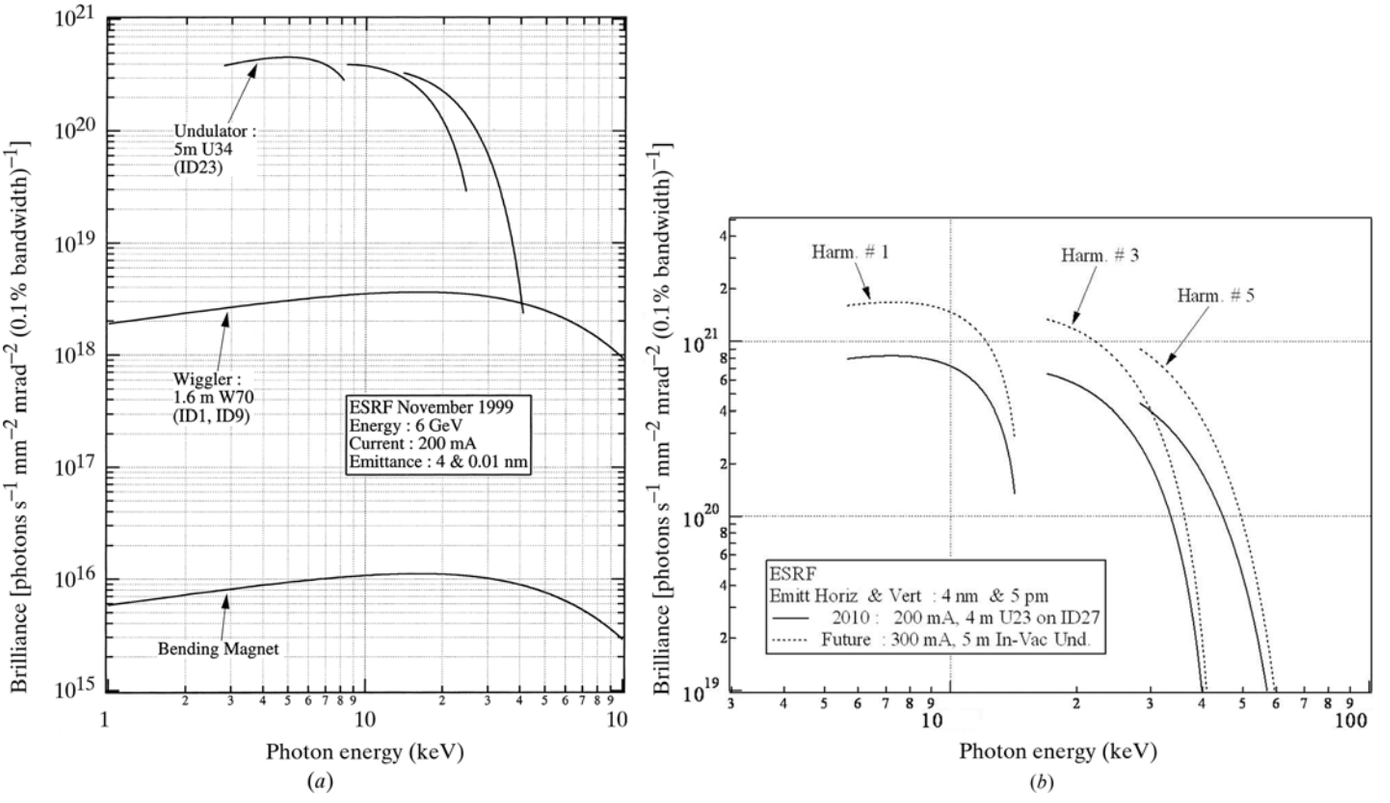


**Figure 8.1.2.2**
SR spectra. (*a*) Spectral brightness (also referred to as brilliance) of different SR source types (undulator, multipole wiggler and bending magnet) as exemplified by such types of sources at the ESRF. For the undulator, the tuning range (*i.e.* as the magnet gap is changed) is indicated. (*b*) Brilliance produced by the in-vacuum undulator of cell 27 of the ESRF dedicated to high-pressure studies. The plain curve corresponds to the condition in use as of September 2010. Further increase in brilliance (dotted curve) is expected in the years to come by increasing the ring current, increasing the length of the undulator and further decreasing the vertical emittance. Kindly provided by Dr Pascal Elleaume, ESRF, Grenoble, France.

units, are so ensconced in the field 'that a drive to change this would only lead to more confusion rather than more clarity in the descriptions of synchrotron-radiation sources'. At the ESRF the term brilliance is firmly ensconced in house and with its large user community, and so is the label for the $y$ axes used in Fig 8.1.2.2.

Another useful term is the machine emittance, $\varepsilon$. This is an invariant for a given machine lattice and electron/positron machine energy. It is the product of the divergence angle, $\sigma'$, and the source size, $\sigma$:

$$\varepsilon = \sigma\sigma'. \tag{8.1.2.2}$$

The horizontal and vertical emittances need to be considered separately.

The total radiated power, $Q$ (kW), is expressed in terms of the machine energy, $E$ (GeV), the radius of curvature of the orbiting electron/positron beam, $\rho$ (m), and the circulating current, $I$ (A), as

$$Q = 88.47E^4 I/\rho. \tag{8.1.2.3}$$

The opening half-angle of the synchrotron radiation is $1/\gamma$ and is determined by the electron rest energy, $mc^2$, and the machine energy, $E$:

$$\gamma^{-1} = mc^2/E. \tag{8.1.2.4}$$

The basic spectral distribution is characterized by the universal curve of synchrotron radiation, which is the number of photons per s per A per GeV per horizontal opening in mrad per 1% $\delta\lambda/\lambda$ integrated over the vertical opening angle, plotted versus $\lambda/\lambda_c$. Here the critical wavelength, $\lambda_c$ (Å), is given by

$$\lambda_c = 5.59\rho/E^3, \tag{8.1.2.5}$$

again with $\rho$ in m and $E$ in GeV. Examples of SR spectral curves are shown in Fig. 8.1.2.2(*a*). The peak photon flux occurs close to $\lambda_c$, the useful flux extends to about $\lambda_c/10$, and exactly half of the total power radiated is above the critical wavelength and half is below this value.

In the plane of the orbit, the beam is essentially 100% plane polarized. This is what one would expect if the electron orbit was visualized edge-on. Away from the plane of the orbit there is a significant (several per cent) perpendicular component of polarization. Schiltz & Bricogne (2009) advocated definitions to use in the analysis of polarization-dependent phenomena that are instrument-independent and completely general. They have implemented these methods in the macromolecular phasing program *SHARP* for exploiting the polarization anisotropy of anomalous scattering in protein crystals.

### 8.1.3. Insertion devices (IDs)

These are multipole magnet devices placed (inserted) in straight sections of the synchrotron or storage ring. They can be designed to enhance specific characteristics of the SR, namely

(1) to extend the spectral range to shorter wavelengths (wavelength shifter);
(2) to increase the available intensity (multipole wiggler);
(3) to increase the spectral brightness *via* interference and also yield a quasi-monochromatic beam (undulator) (Fig. 8.1.2.2*b* shows the distinctly different emission from an undulator);

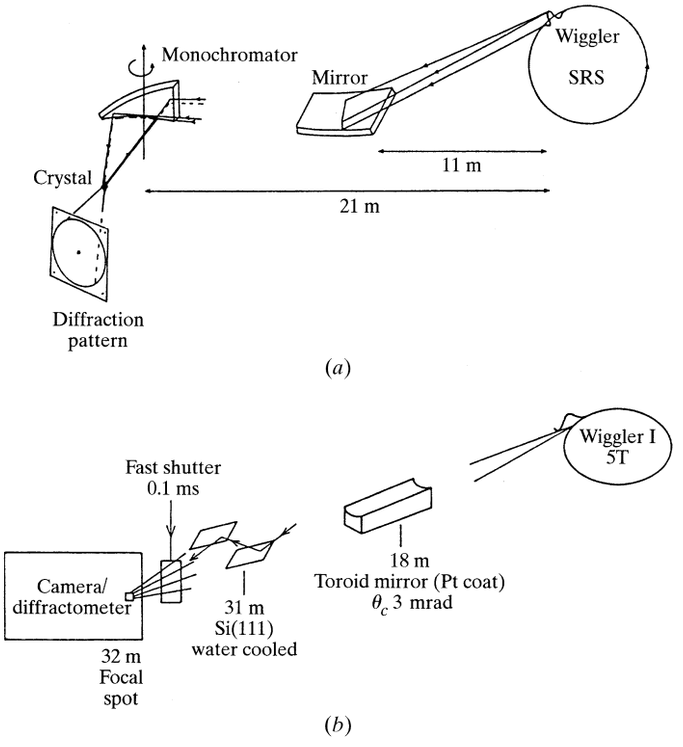


**Figure 8.1.4.1**
Common beamline optics modes. (*a*) Horizontally focusing cylindrical monochromator and vertical focusing mirror [shown here for station 9.6 as existed at the SRS (adapted from Helliwell *et al.*, 1986)]. (*b*) Rapidly tunable double-crystal monochromator and point-focusing toroid mirror [shown here as existed for station 9.5 at the SRS (adapted from Brammer *et al.*, 1988)].

(4) to provide a different polarization (*e.g.* to rotate the plane of polarization, to produce circularly polarized light *etc.*).

The classification of a periodic magnet ID as a wiggler or undulator is based on whether the angular deflection, $\delta$, of the electron beam is small enough to allow radiation emitted from one pole to interfere directly with that from the next pole. In a wiggler, $\delta \gg \gamma^{-1}$, so the interference is negligible and the spectral emission (Fig. 8.1.2.2*a*) is very similar in shape to, but scaled up from, the universal curve (*i.e.* bending magnet spectral shape). In an undulator $\delta \leq \gamma^{-1}$ and the interference effects are highly significant (Fig. 8.1.2.2*b*). If the period of the ID is $\lambda_u$ (cm), then the wavelengths $\lambda_i$ ($i$ integer) emitted are given by

$$\lambda_i = \frac{\lambda_u}{i2\gamma^2}\left(1 + \frac{K^2}{2} + \gamma^2\theta^2\right), \qquad (8.1.3.1)$$

where $K = \gamma\delta$.

The spectral width of each peak is

$$\Delta_i \simeq 1/iN, \qquad (8.1.3.2)$$

where $N$ is the number of poles. The angular deflection, $\delta$, is changed by opening or closing the gap between the pole pieces.

### 8.1.4. Beam characteristics delivered at the crystal sample

The sample acceptance, $\alpha$ [equation (8.1.4.1)], is a quantity to which the synchrotron machine emittance [equation (8.1.2.2)] should be matched, *i.e.*,

$$\alpha = x\eta, \qquad (8.1.4.1)$$

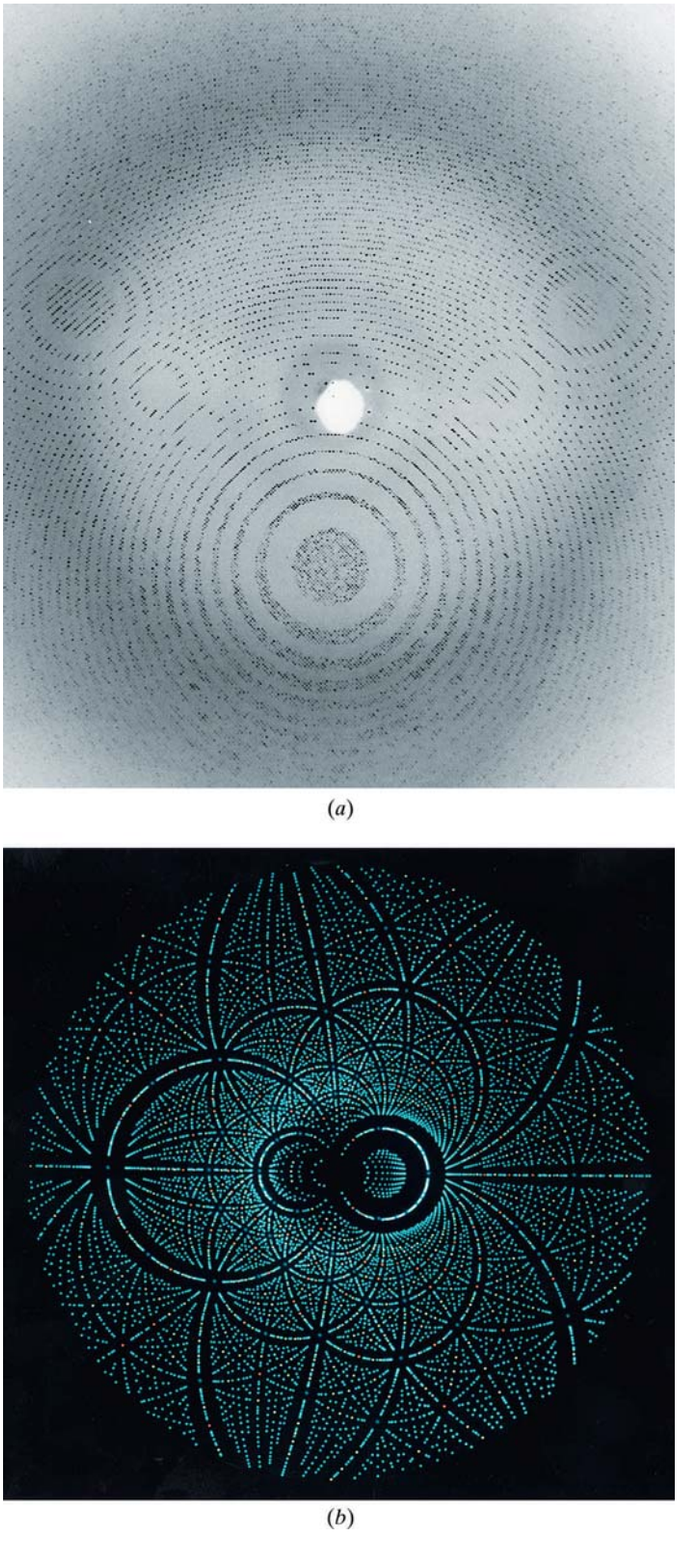


**Figure 8.1.4.2**
Single-crystal SR diffraction patterns. (*a*) Rhinovirus monochromatic oscillation photograph recorded at CHESS (Arnold *et al.* 1987; see also Rossmann & Erickson, 1983). (*b*) Prediction of a protein crystal Laue diffraction pattern (for an illuminating bandpass, without monochromator, $\sim 0.4 < \lambda < 2.6$ Å). The colour coding is according to the multiplicity of each spot: turquoise for singlet reflections, yellow for doublets, orange for triplets and blue for quartet or higher-multiplicity Laue spots (Cruickshank *et al.*, 1991).

where $x$ is the sample size and $\eta$ the mosaic spread. For example, if $x = 0.1$ mm and $\eta = 1$ mrad (0.057°), then $\alpha = 10^{-7}$ m rad or 100 nm rad.

**Table 8.1.4.1**
Internet addresses of SR facilities with macromolecular crystallography beamlines

| Synchrotron-radiation source | Location | Address |
|---|---|---|
| ALS, Advanced Light Source | Lawrence Berkeley Lab., Berkeley, California, USA | http://www-als.lbl.gov/als/ |
| ANKA Synchrotron | Karlsruhe, Germany | http://ankaweb.fzk.de/ |
| APS, Advanced Photon Source | Argonne National Lab., Chicago, Illinois, USA | http://epics.aps.anl.gov/ |
| Australian Synchrotron | Clayton, Victoria, Australia | http://www.synchrotron.org.au/ |
| BESSY | Berlin, Germany | http://www.bessy.de/ |
| Brazilian Synchrotron Light Laboratory | Campinas, Brazil | http://www.lnls.br/ |
| BSRF, Beijing Synchrotron Radiation Facility | Beijing, China | http://www.ihep.ac.cn/bsrf/english/main/main.htm |
| CAMD, Center for Advanced Microstructures and Devices | Baton Rouge, Louisiana, USA | http://www.camd.lsu.edu/ |
| Canadian Light Source | Saskatoon, Canada | http://www.lightsource.ca/ |
| CHESS, Cornell High Energy Synchrotron Source | Ithaca, New York, USA | http://www.chess.cornell.edu/ |
| Diamond Light Source | Harwell Science and Innovation Campus, Didcot, England | http://www.diamond.ac.uk/ |
| Elettra | Trieste, Italy | http://www.elettra.trieste.it |
| ESRF, European Synchrotron Radiation Facility | Grenoble, France | http://www.esrf.fr/ |
| HASYLAB DESY, Deutsches Elektronen-Synchrotron | Hamburg, Germany | http://www.desy.de/ |
| Kurchatov Center for Synchrotron Radiation and Nanotechnology | Moscow, Russian Federation | http://www.kcsr.kiae.ru/en/ |
| LNLS, National Synchrotron Light Laboratory | Campinas, Brazil | http://www.lnls.br/ |
| MAXLab (see also MAX IV project) | Lund, Sweden | http://www.maxlab.lu.se/, http://www.maxlab.lu.se/maxlab/max4/index.html |
| NSLS, National Synchrotron Light Source (see also NSLS II; under construction) | Brookhaven National Lab., New York, USA | http://www.nsls.bnl.gov/, http://www.bnl.gov/nsls2/ |
| The Photon Factory, KEK | Tsukuba, Japan | http://pfwww.kek.jp/ |
| PLS, Pohang Light Source | Pohang, Korea | http://pal.postech.ac.kr/ |
| SESAME (Synchrotron-light for Experimental Science and Applications in the Middle East) | Allan, Jordan | http://www.sesame.org.jo/ |
| Shanghai Synchrotron Radiation Facility | Shanghai, China | http://ssrf.sinap.ac.cn/english/1/Introduction.htm |
| SLS, Swiss Light Source | Paul Scherrer Institut, Villigen, Switzerland | http://sls.web.psi.ch/view.php/about/index.html |
| Soleil | Gif-sur-Yvette, Paris, France | http://www.synchrotron-soleil.fr/portal/page/portal/Accueil |
| SPring-8, Super Photon Ring | Riken Go, Japan | http://www.spring8.or.jp/ |
| SRRC, Synchrotron Radiation Research Center | Hsinchu City, Taiwan | http://www.nsrrc.org.tw/ |
| SSRL, Stanford Synchrotron Radiation Laboratory | SLAC, California, USA | http://www-ssrl.slac.stanford.edu/ |
| VEPP-3 | Novosibirsk, Russia | http://ssrc.inp.nsk.su/ |

At the sample position, the intensity of the beam, usually focused, is a useful parameter:

$$\text{Intensity} = \text{photons per s per focal spot area.} \qquad (8.1.4.2)$$

Moreover, the horizontal and vertical convergence angles are ideally kept smaller than the mosaic spread, *e.g.* ~1 mrad, so as to measure reflection intensities with optimal peak-to-background ratio.

Producing a focal spot area that is approximately the size of a typical crystal (~0.1 mm) and with a convergence angle ~1 mrad sets a sample acceptance requirement to be met by the X-ray beam and machine emittance. A machine with an emittance that matches the acceptance of the sample greatly assists the simplicity and performance of the beamline optics (mirror and/or monochromator) design. The common beamline optics schemes are shown in Fig. 8.1.4.1.

In addition to the focal spot area and convergence angles, it is necessary to provide the appropriate spectral characteristics. In monochromatic applications, involving the rotating-crystal diffraction geometry, for example, a particular wavelength, $\lambda$, and narrow spectral bandwidth, $\delta\lambda/\lambda$, are used. Fig. 8.1.4.2(*a*) shows an example of a monochromatic oscillation diffraction photograph from a rhinovirus crystal as an example recorded at CHESS, Cornell. Fig. 8.1.4.2(*b*) shows the prediction of a white-beam broad-band Laue diffraction pattern from a protein crystal that was recorded at the SRS wiggler, Daresbury, colour-coded for multiplicity.

Table 8.1.4.1 lists the internet addresses of the SR facilities worldwide that currently have macromolecular beamlines. A considerable suite of information on SR and free electron laser (FEL) sources can also be found at http://www.lightsources.org/cms/. Comprehensive statistics for the macromolecular crystal structures from all the various beamlines over the years can be obtained at http://biosync.rcsb.org/.

### 8.1.5. Evolution of SR machines and experiments

#### *8.1.5.1. First-generation SR machines*

The so-called first generation of SR machines were those which were parasitic on high-energy physics operations, such as DESY in Hamburg, SPEAR in Stanford, NINA in Daresbury and VEPP in Novosibirsk. These machines had high fluxes into the X-ray range and enabled pioneering experiments. Parratt (1959) discussed the use of the CESR (Cornell Electron Storage Ring) for X-ray diffraction and spectroscopy in a very perceptive paper. Cauchois *et al.* (1963) conducted *L*-edge absorption spectroscopy at Frascati and were the first to diffract SR with a crystal (quartz). The opening experimental work in the area of biological diffraction was by Rosenbaum *et al.* (1971). In protein crystallography, multiple-wavelength anomalous-dispersion effects (Fig.

8.1.5.1) were used from the onset (Phillips *et al.*, 1976, 1977; Phillips & Hodgson, 1980; Webb *et al.*, 1977; Harmsen *et al.*, 1976; Helliwell, 1977, 1979), and a reduction in radiation damage was seen for high-resolution data collection (Wilson *et al.*, 1983). Historical insights into the performances of those machines, from the current-day perspective, are described in detail, for example, by Huxley & Holmes (1997) at DESY, Munro (1997) at Daresbury, and Doniach *et al.* (1997) at Stanford. A principal limitation was the problem of source movements, which degraded the focusing of the source onto a small crystal or single fibre and thus degraded the intrinsic spectral brightness of the beam; see, for example, Haslegrove *et al.* (1977), who advocated machine shifts dedicated to SR as a working compromise with the high-energy physicists. Some possible applications that were discussed were unfulfilled until brighter sources became available. The two-wavelength crystallography phasing method of Okaya & Pepinsky (1956) (see also Hoppe & Jakubowski, 1975) and the three-wavelength method of Herzenberg & Lau (1967), as well as the implementation of the algebraic method of Karle (1967, 1980, 1989, 1994), awaited more stable beams, which had to be rapidly and easily tunable over a fine bandpass (ideally $10^{-4}$). Experiments to define the anomalous-dispersion coefficients, including dichroism effects, at a large number of wavelengths at several example absorption edges in a variety of crystal structures were conducted at SPEAR (Phillips *et al.*, 1978; Templeton *et al.*, 1980, 1982; Templeton & Templeton, 1985). Large values of $f''$ were identified at 'white lines', *i.e.* regions of the elemental absorption with pronounced effects (*e.g.* see Fig 8.1.5.1*a*). Values of $f'$ over a continuum of wavelengths in a real compound (*i.e.*, not a metal in the gas phase) (Fig. 8.1.5.1*b*) were explored in a profile approach (now called DAFS, diffraction anomalous fine structure) by Arndt *et al.* (1982) at the newly commissioned SRS, the first dedicated second-generation SR source (see Section 8.1.5.2).

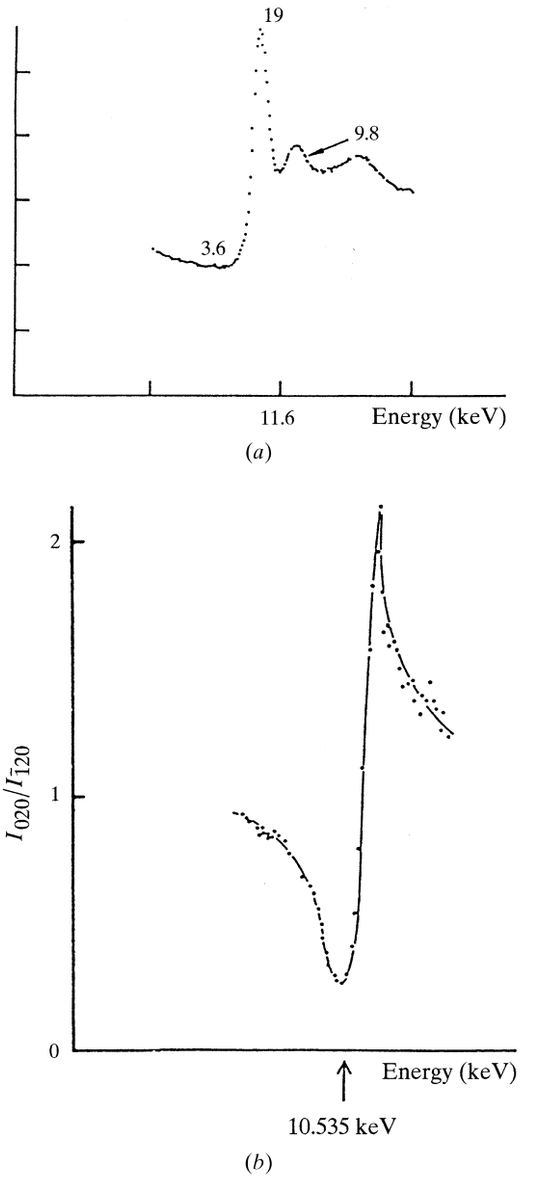


**Figure 8.1.5.1**
Anomalous dispersion. (*a*) $f''$ as represented by an absorption spectrum [Pt $L_{III}$ edge for $K_2Pt(CN)_4$ as the example with 19 electrons for $f''$ at the peak of that 'white line', with pre-edge and post-edge $f''$ electron values also indicated] (Helliwell, 1984). Reproduced with the permission of the Institute of Physics. (*b*) $f'$ as estimated by a continuous polychromatic profile method. Reproduced with permission from *Nature* (Arndt *et al.*, 1982). Copyright (1982) MacMillan Magazines Limited.

### *8.1.5.2. Second-generation dedicated machines*

The building of dedicated X-ray sources began with the SRS at Daresbury, which came online in 1980, having followed the NINA synchrotron (closed in 1976) and the associated Synchrotron Radiation Facility at Daresbury. Elsewhere in the world, LURE (Lemonnier *et al.*, 1978) and CHESS at Cornell were building up their SR macromolecular crystallography operations in the late 1970s and early 1980s, and the NSLS in Brookhaven and the Photon Factory (PF) in Japan were both under construction. The NSLS and the PF came online in 1983 and 1984, respectively. Thus, there was a rapid increase in the number of operating machines and beamlines worldwide in the X-ray region for protein crystallography. There were teething problems with the SRS with the radio-frequency cavity window problem, interrupting operation for many months in 1983, and at the NSLS in its early period due to vacuum-chamber problems. Pioneering experiments continued and blossomed. Seminal work ensued in virus crystallography [Rossmann & Erickson (1983) at Hamburg and Daresbury; and Usha *et al.* (1984) at LURE], Laue diffraction for time-resolved protein crystallography [Moffat *et al.* (1984) at CHESS; Helliwell (1984, 1985) at the SRS; Cruickshank *et al.* (1987, 1991); Hajdu, Machin *et al.* (1987); Helliwell *et al.* (1989); Bourenkov *et al.* (1996); Neutze & Hajdu (1997)], enzyme catalysis in the crystal [Hajdu, Acharya *et al.* (1987) at the SRS], MAD [Phillips *et al.* (1977); Einspahr *et al.* (1985); Hendrickson (1985); Hendrickson *et al.* (1989) at SPEAR, the SRS and the PF; Guss *et al.* (1988) at SPEAR; Kahn *et al.* (1985) at LURE; Korszun (1987) at CHESS; Mukherjee *et al.* (1989) and Peterson *et al.* (1996) at the SRS; Hädener *et al.* (1999) at the SRS and the ESRF, to cite a few experiments], protein crystallography involving isomorphous replacement with optimized anomalous scattering [Baker *et al.* (1990) at the SRS; Dumas *et al.* (1995) at LURE], small crystals [Hedman *et al.* (1985) at the SRS] and diffuse scattering with SR [Doucet & Benoit (1987); Caspar *et al.* (1988); Glover *et al.* (1991)]. Table 8.1.5.1 shows the impact of the SRS in protein (*i.e.* macromolecular) crystallography integrated over its whole lifetime.

### *8.1.5.3. Third-generation high spectral brightness machines*

As early as 1979, there were discussions on planning a proposal for a high spectral brightness, insertion-device-driven European synchrotron-radiation (ESR) source. A wide variety of discussion

**Table 8.1.5.1**
Structures in the Protein Data Bank (PDB) for which data were collected at the SRS

The data presented here were compiled in December 2009 (see http://biosync.rcsb.org/biosync_regions/SyncEurope.html#SRS) and are likely to be reasonably complete since the SRS closed operations in August 2008. The SRS has delivered 3.6% of the total of 38 650 macromolecular crystal structures determined using radiation from synchrotrons around the world as of December 2009. The ESRF third-generation source, in comparison, integrated over about half as many years, but about two to three times more beamlines, has delivered 15.6% of the structures, *i.e.* at a rate therefore about three to four times greater than the second-generation SRS.

| | Station | | | | | | |
|---|---|---|---|---|---|---|---|
| Year | 10.1 | 14.1 | 14.2 | 7.2 | 9.5 | 9.6 | Not known |
| 1995 | 0 | 0 | 0 | 5 | 6 | 19 | 3 |
| 1996 | 0 | 0 | 0 | 6 | 11 | 33 | 0 |
| 1997 | 0 | 0 | 0 | 11 | 29 | 43 | 0 |
| 1998 | 0 | 0 | 0 | 26 | 32 | 35 | 0 |
| 1999 | 0 | 0 | 0 | 28 | 13 | 45 | 4 |
| 2000 | 0 | 1 | 0 | 28 | 17 | 60 | 3 |
| 2001 | 0 | 13 | 9 | 9 | 16 | 47 | 2 |
| 2002 | 0 | 13 | 21 | 7 | 7 | 59 | 2 |
| 2003 | 0 | 27 | 38 | 3 | 8 | 41 | 3 |
| 2004 | 3 | 40 | 42 | 5 | 2 | 36 | 2 |
| 2005 | 18 | 34 | 36 | 1 | 4 | 47 | 1 |
| 2006 | 22 | 32 | 22 | 1 | 1 | 23 | 0 |
| 2007 | 21 | 37 | 21 | 0 | 0 | 11 | 1 |
| 2008 | 51 | 15 | 15 | 2 | 0 | 20 | 1 |
| 2009 | 14 | 12 | 5 | 1 | 0 | 3 | 0 |
| Total | 129 | 224 | 209 | 133 | 146 | 522 | 22 |

documents and workshops, and the ESR Project (ESRP) led by B. Buras and based in Geneva at CERN, culminated in the so-called 'Red Book' in 1987, the *ESRF Foundation Phase Report* (1987), totalling some 1000 pages of machine, beamline and experimental specifications and costs. This, then, was the progenitor of the third-generation sources, characterized by their high energy and high spectral brightness, tailored to optimized undulator emission in the 1 Å range. Actually, the ESRF machine energy was initially set at 5 GeV, but increased to 6 GeV to optimize the production of 14.4 keV photons to better match the nuclear scattering experiments proposed initially by Mossbauer in 1975. Proposals for the US machine, the Advanced Photon Source at 7 GeV, and the Japanese 8 GeV SPring-8 machine followed, with the higher machine energy enhancing the X-ray tuning range of undulators. Thus, MAD tuning-based techniques were facilitated with these machines and studies involving yet-smaller samples (crystals, single fibres or tiny liquid aliquots) or very large unit cells were enabled. As a result, micron-sized protein crystals as well as huge multi-macromolecular biological structures (of large viruses, for example) also became routinely accessible.

*8.1.5.4. New national SR machines*

Today a variety of enhanced national SR machines have been built. In Switzerland there is the SLS, in the UK there is DIAMOND and in France there is SOLEIL. These machines are more tailored to the bulk of a country's user needs, distinct from the special provisions at the ESRF. The different countries' SR needs, of course, have many aspects in common, with some historical biases. The new sources are, in essence, characterized by high spectral brightness, *i.e.*, low emittance. The 2 GeV SR source ELETTRA in Trieste, the MAXII machine in LUND and the Brazilian Light Source are already operational. In many ways, national sources like the SRS, LURE, DORIS and so on fuelled the case and specification for the ESRF. Now the developments at the ESRF, including high harmonic emission of undulators *via* magnet shimming (Elleaume, 1989) and narrow-gap undulator operation (Elleaume, 1998), are fuelling ideas and the specification of what is possible in the new national SR sources.

*8.1.5.5. X-ray free-electron lasers (XFELs)*

In terms of the evolution of X-ray sources, X-ray FELs are being constructed at DESY in Hamburg (Brinkmann *et al.*, 1997), at SLAC (Winick, 1995) and at Spring8. Compared to SR, one will have a transversely fully coherent beam, a larger average spectral brightness and, in particular, pulse lengths of ~10 fs full width at half-maximum with eight to ten orders of magnitude larger peak spectral brightness. Such a machine is based on a linear accelerator (linac)-driven XFEL utilizing a linear collider installation (*e.g.*, for a high-energy physics centre-of-mass energy capability of 500 GeV). For this machine there is a 'switchyard' distributing the electrons in a beam to different undulators from which the X-rays are generated in the range 0.1 to ~12 keV. The anticipated r.m.s. opening angle would be 1 mrad and the source diameter would be 20 μm. This source of X-rays would then compete in time resolution with laser-pulse-generated X-ray beams [see Helliwell & Rentzepis (1997) for a survey of that work and a comparison with synchrotron radiation] and would also have higher pulse flux. Coherent methods in the X-ray sciences have been extensively reviewed by Nugent (2009).

### 8.1.6. SR instrumentation

The divergent continuum of X-rays from the source must be intercepted by the sample cross-sectional area. The crystal sample acceptance, as seen above, is a good way to illustrate to the machine designer the sort of machine emittances required. Likewise, the beamline optics, mirrors and monochromators should not degrade the X-ray beam quality. Mirror surface and shape finish have improved a great deal in the last few decades; slope errors of mirrors, even for difficult shapes like polished cylinders, which on bending give a toroidal reflecting surface, are now around 1 arc second (5.5 μrad) for a length of 1 m. Thus, over focusing distances of 10–20 m, say, the focal-spot smearing contribution from this is 55–110 μm, important for focusing onto small crystals. Further optics developments (*e.g.* Fresnel optics) have yielded micron focus beams and smaller, and are being applied to studying ever-smaller crystals in macromolecular crystallography and obviously have a variety of other diffraction

and spectroscopy applications [for a review, see Riekel (2000)]. The choice of materials has evolved, too, from the relatively easy-to-work-with and -finish fused quartz to silicon; silicon having the advantageous property that at liquid-nitrogen temperature the expansion coefficient is zero (Bilderback, 1986). This has been of particular advantage in the cooling of silicon monochromators at the ESRF, where the heat loading on optics is very high. An alternative approach with the rather small X-ray beams from undulators is the use of transparent monochromator crystals made of diamond, which is a robust material with the additional advantage of transparency, thus allowing multiplexing of stations, one downstream from the other, fed by one straight section of one or more undulator designs. For a review of the ESRF beamline optics, see Freund (1996); for reviews of the macromolecular crystallography programmes at the ESRF, see Miller (1994), Branden (1994) and Lindley (1999), as well as the *ESRF Foundation Phase Report* (1987). See also Helliwell (1992), Chapter 5.

Detectors have improved enormously. The early days of SR use saw considerable reliance on photographic film, as well as single-counter four-circle diffractometers. Evolution of area detectors, in particular, has been considerable and impressive, and in a variety of technologies. Gas detectors, *i.e.*, the multiwire proportional chamber (MWPC), were invented and developed through various generations and types [Charpak (1970); for reviews of their use at SR sources, see *e.g.* Lewis (1994) and Fourme (1997)]. MWPCs have the best detector quantum efficiency (DQE) of the area detectors, but there are limitations on count rate (local and global) and their use at wavelengths less than ~1 Å is restricted due to geometric image parallax effects. The most popular devices at present are charge coupled devices (CCDs) [see Tate *et al.* (1995), Allinson (1994), Gruner & Ealick (1995) and Westbrook & Naday (1997) for details of their development]. Image plates (IPs) were popular during the late 1980s and early to mid-1990s, mainly, but not exclusively, with online scanners, notably the MAR Research devices. IPs are also used in a Weissenberg geometry [see Sakabe (1983, 1991) and Sakabe *et al.* (1995), and for a recent review see Amemiya (1997)]. IPs and CCDs are complementary in performance, especially with respect to size and duty cycle; IPs are larger, *i.e.*, with many resolution elements possible, but are slower to read out than CCDs. Both are capable of imaging well at wavelengths shorter than 1 Å and with high count rates. Both have overcome the tedium of chemical development of film. Other detectors needed for crystallography include those for monitoring the beam intensity; these must not interfere with the beam collimation, and yet must monitor the beam downstream of the collimator (Bartunik *et al.*, 1981); also needed are fluorescence detectors for setting the wavelength for optimized anomalous-scattering applications (see Cianci *et al.*, 2005).

Most recently, an area-detector development has been the so-called pixel detector. This is made of silicon cells, each 'bump bonded' onto associated individual electronic readout chains. Thus, extremely high count rates are possible. These devices can then combine the attributes of large image plate sensitive areas with the fast readout of CCDs, along with high count-rate capability and so on. Devices and prototypes have been developed at Princeton/Cornell (Eikenberry *et al.*, 1998), Berkeley/San Diego (Beuville *et al.* 1997) and Imperial College, London (Hall, 1995), and are now in use at the SLS (Broennimann *et al.*, 2006).

Provision of robotics for sample mounting on the synchrotron beamlines has been increasingly deployed in the last decade, improving efficiency and ease of use, often coupled with remote access (*e.g.* see Gonzalez *et al.*, 2005) and telepresence (*e.g.* see Warren *et al.*, 2008).

### 8.1.7. SR monochromatic and Laue diffraction geometry

In the utilization of SR, both Laue and monochromatic modes are important for data collection. The unique geometric and spectral properties of SR render the treatment of diffraction geometry different from that for a conventional X-ray source.

#### *8.1.7.1. Laue geometry: sources, optics, sample reflection bandwidth and spot size*

Laue geometry involves the use of the polychromatic SR spectrum as transmitted through the beryllium window that is used to separate the apparatus from the machine vacuum. There is useful intensity down to a wavelength minimum of $\sim\lambda_c/5$, where $\lambda_c$ is the critical wavelength of the magnet source in the case of bending magnets (BMs) and wavelength shifters. The maximum wavelength is typically $\geq$3 Å; however, if the crystal is mounted in a capillary, then the glass absorbs the wavelengths beyond ~2.5 Å (Helliwell, 2004).

The bandwidth on BMs and wigglers can be limited by a reflecting mirror at grazing incidence, whereby the minimum wavelength in the beam can be sharply defined to aid the accurate definition of the Laue spot multiplicity. The mirror can also be used to focus the beam at the sample. The maximum-wavelength limit can be truncated by use of aluminium absorbers of varying thickness or a transmission mirror (Lairson & Bilderback, 1982; Cassetta *et al.*, 1993).

The measured intensity of individual Laue diffraction spots depends on the wavelength at which they are stimulated. The problem of wavelength normalization is treated by a variety of methods. These include:

(i) use of a monochromatic reference data set;
(ii) use of symmetry equivalents and multiple measurements in the Laue data set recorded at different wavelengths;
(iii) calibration with a standard sample, such as a silicon crystal.

Each of these methods produces a 'λ curve' describing the relative strength of spots measured at various wavelengths. Most Laue diffraction data are now recorded on CCDs or IPs. The greater sensitivity of these detectors (expressed as the DQE), especially for weak signals, has greatly increased the number of Laue exposures recordable per crystal (*e.g.* Nieh *et al.*, 1999). Thus, multiplet deconvolution procedures, based on the recording of reflections stimulated at different wavelengths and with different relative intensities, have become possible (Campbell & Hao, 1993; Ren & Moffat, 1995*b*; Nieh *et al.*, 1999). Data quality and completeness have improved considerably.

Narrow-bandpass beams, *e.g.* $\delta\lambda/\lambda \leq 0.2$, are used for enhancing the signal-to-noise ratio. Such bandwidths are produced generally by an X-ray undulator, whereby *e.g.* 10–100 periods should ideally yield a bandwidth behind a pinhole of $\delta\lambda/\lambda \simeq 0.1$–0.01. In these cases, wavelength normalization is more difficult, because the actual spectrum over which a reflection is integrated is rapidly varying in intensity; nevertheless, high-order Chebychev polynomials are successful (Ren & Moffat, 1995*a*; Artz *et al.*, 1999).

The spot bandwidth is determined by the mosaic spread and horizontal beam divergence (since $\gamma_H > \gamma_V$) as

$$(\delta\lambda/\lambda) = (\eta + \gamma_H)\cot\theta, \qquad (8.1.7.1)$$

where $\eta$ is the sample mosaic spread, assumed to be isotropic, and

$\gamma_H$ is the horizontal cross-fire angle, which in the absence of focusing is $(x_H + \sigma_H)/P$, where $x_H$ is the horizontal sample size, $\sigma_H$ is the horizontal source size and $P$ is the sample to the tangent-point distance. This is similar for $\gamma_V$ in the vertical direction. Generally, at SR sources, $\sigma_H$ is greater than $\sigma_V$. When a focusing-mirror element is used, $\gamma_H$ and/or $\gamma_V$ are convergence angles determined by the focusing distances and the mirror aperture.

The size and shape of the diffraction spots vary across the detector image plane. The radial spot length is given by convolution of Gaussians as

$$\left(L_R^2 + L_c^2 \sec^2 2\theta + L_{\rm PSF}^2\right)^{1/2} \qquad (8.1.7.2)$$

and tangentially by

$$\left(L_T^2 + L_c^2 + L_{\rm PSF}^2\right)^{1/2}, \qquad (8.1.7.3)$$

where $L_c$ is the size of the X-ray beam (assumed to be circular) at the sample, $L_{\rm PSF}$ is the detector point-spread factor,

$$L_R = D \sin(2\eta + \gamma_R) \sec^2 2\theta, \qquad (8.1.7.4)$$

$$L_T = D(2\eta + \gamma_T) \sin\theta \sec 2\theta, \qquad (8.1.7.5)$$

and

$$\gamma_R = \gamma_V \cos\psi + \gamma_H \sin\psi, \qquad (8.1.7.6)$$

$$\gamma_T = \gamma_V \sin\psi + \gamma_H \cos\psi, \qquad (8.1.7.7)$$

where $\psi$ is the angle between the vertical direction and the radius vector to the spot (see Andrews *et al.*, 1987). For a crystal that is not too mosaic, the spot size is dominated by $L_c$ and $L_{\rm PSF}$. For a mosaic or radiation-damaged crystal, the main effect is a radial streaking arising from $\eta$, the sample mosaic spread.

### *8.1.7.2. Monochromatic SR beams: optical configurations and sample rocking width*

A wide variety of perfect-crystal monochromator configurations are possible and have been reviewed by various authors (Hart, 1971; Bonse *et al.*, 1976; Hastings, 1977; Kohra *et al.*, 1978). Since the reflectivity of perfect silicon and germanium is effectively 100%, multiple-reflection monochromators are feasible and permit the tailoring of the shape of the monochromator resolution function, harmonic rejection and manipulation of the polarization state of the beam. Two basic designs are in common use. These are the bent single-crystal monochromator of triangular shape (Fig. 8.1.4.1*a*) and the double-crystal monochromator (Fig. 8.1.4.1*b*).

#### *8.1.7.2.1. Curved single-crystal monochromator*

In the case of the single-crystal monochromator, the actual curvature employed is very important in the diffraction geometry. For a point source and a flat monochromator crystal, there is a gradual change in the photon wavelength selected from the white beam as the length of the monochromator is traversed (Fig. 8.1.7.1*a*). For a point source and a curved monochromator crystal, one specific curvature can compensate for this variation in incidence angle (Fig. 8.1.7.1*b*). The reflected spectral bandwidth is then at a minimum; this setting is known as the 'Guinier position'. If the curvature of the monochromator crystal is increased further, a range of photon wavelengths, $(\delta\lambda/\lambda)_{\rm corr}$, is selected along its length so that the rays converging towards the focus have a correlation of photon wavelength and direction (Fig. 8.1.7.1*c*). The effect of a finite source is to cause a change in incidence angle at the monochromator crystal, so that at the focus there is a photon-wavelength gradient across the width of the focus (for all curvatures) (Fig. 8.1.7.1*d*). The use of a slit in the focal plane is akin to placing a slit at the tangent point to limit the source size.

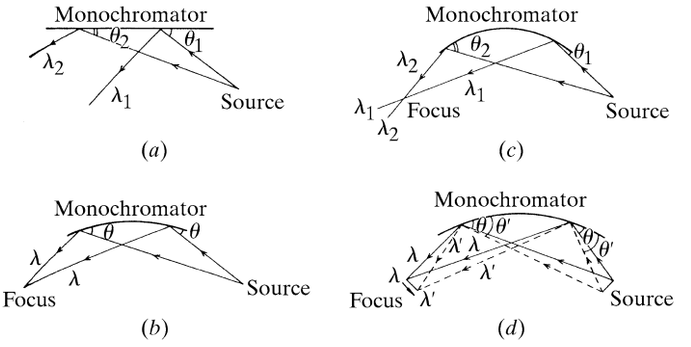


**Figure 8.1.7.1**
Single-crystal monochromator illuminated by SR. (*a*) Flat crystal. (*b*) Guinier setting. (*c*) Overbent crystal. (*d*) Effect of source size (shown at the Guinier setting for clarity). From Helliwell (1984). Reproduced with the permission of the Institute of Physics.

#### *8.1.7.2.2. Double-crystal monochromator*

The double-crystal monochromator with two parallel or nearly parallel perfect crystals of germanium or silicon is a common configuration. The advantage of this is that the outgoing monochromatic beam is parallel to the incoming beam, although it is slightly displaced vertically by an amount $2d\cos\theta$, where $d$ is the perpendicular distance between the crystals and $\theta$ is the monochromator Bragg angle (unless the second crystal is unconnected to the first, in which case it can be translated as well to compensate for that). The monochromator can be rapidly tuned, since the diffractometer or camera need not be re-aligned significantly in a scan across an absorption edge. Since the rocking width of the fundamental is broader than the harmonic reflections, the strict parallelism of the pair of the crystal planes can be 'detuned', so that the harmonic can be rejected with little loss of the fundamental intensity. The spectral spread in the reflected monochromatic beam is determined by the source divergence accepted by the monochromator, the angular size of the source and the monochromator rocking width (see Fig. 8.1.7.2). The double-crystal monochromator is often used with a toroidal focusing mirror; the functions of monochromatization are then separated from the focusing (Hastings *et al.*, 1978).

#### *8.1.7.2.3. Widening of monochromatic wavelength range provision*

Users and facilities have been driven to use an ever-widening practical range of X-ray wavelengths. Longer wavelengths in protein crystallography have been explored up to 2.6 Å (Helliwell, 1993, 1997*a*, 2004; Polikarpov *et al.*, 1997; Teplyakov *et al.*, 1998; Cianci *et al.*, 2001, 2008), and even softer wavelengths have been under active development to utilize the uranium *M* edge at 3.326 and 3.490 Å (Liu *et al.*, 2001), and the S *K* edge for anomalous dispersion (Stuhrmann & Lehmann, 1994). At very short (~0.5 Å) and ultra-short (~0.3 Å) wavelengths, a high machine energy yields copious flux output; pilot studies have been conducted in protein crystallography at CHESS (Helliwell *et al.*, 1993), at the ESRF (Schiltz *et al.*, 1997) and at the NSLS (Jakoncic *et al.*, 2006). Notably Fourme and colleagues have exploited the condensed angular distribution of the diffraction pattern at such wavelengths to pass the beam through the narrow

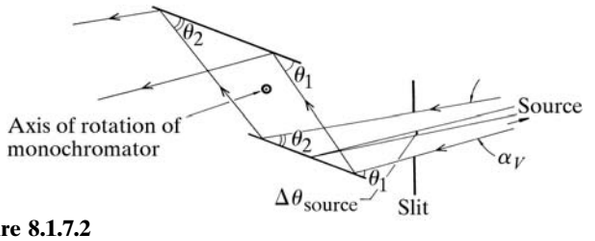


**Figure 8.1.7.2**
Double-crystal monochromator illuminated by SR. The contributions of the source divergence, $\alpha_V$ [less than or equal to $\gamma^{-1}$, equation (8.1.2.4), depending on the monochromator vertical entrance slit aperture; see also Colapietro *et al.* (1992)], and angular source size, $\Delta\theta_{\text{source}}$, to the range of energies reflected by the monochromator are shown. From Helliwell (1984). Reproduced with the permission of the Institute of Physics.

exit window of a high-pressure cell for protein-crystal high-pressure biophysical studies (Fourme *et al.*, 2001; Girard *et al.*, 2007). Such developments interact closely with machine and beamline specifications.

*8.1.7.2.4. Crystal sample rocking width*

The rocking width of a reflection depends on the horizontal and vertical beam divergence or convergence (after due account for collimation is taken), $\gamma_H$ and $\gamma_V$, the spectral spreads $(\delta\lambda/\lambda)_{\text{conv}}$ and $(\delta\lambda/\lambda)_{\text{corr}}$, and the mosaic spread, $\eta$. We assume that the mosaic spread $\eta$ is $\gg \omega$, the angular broadening of a reciprocal-lattice point (relp) due to a finite sample. In the case of synchrotron radiation, $\gamma_H$ and $\gamma_V$ are usually widely asymmetric. On a conventional source, usually $\gamma_H \simeq \gamma_V$. Two types of spectral spread occur with synchrotron (and neutron) sources. The term $(\delta\lambda/\lambda)_{\text{conv}}$ is the spread that is passed down each incident ray in a divergent or convergent incident beam; the subscript refers to the conventional source type. This is because it is similar to the $K\alpha_1, K\alpha_2$ line widths and separation. At the synchrotron, this component also exists and arises from the monochromator rocking width and finite-source-size effects. The term $(\delta\lambda/\lambda)_{\text{corr}}$ is special to the synchrotron or neutron case. The subscript 'corr' refers to the fact that the ray direction can be correlated with the photon or neutron wavelength. In this most general case, and for one example of a $(\delta\lambda/\lambda)_{\text{corr}}$ arising from the horizontal ray direction correlation with photon energy and the case of a horizontal rotation axis, the rocking width $\varphi_R$ of an individual reflection is given by

$$\varphi_R = \left\{L^2\left[(\delta\lambda/\lambda)_{\text{corr}} d^{*2} + \zeta\gamma_H\right]^2 + \gamma_V^2\right\}^{1/2} + 2\varepsilon_s L, \qquad (8.1.7.8)$$

where

$$\varepsilon_s = (d^* \cos\theta/2)\left[\eta + (\delta\lambda/\lambda)_{\text{conv}} \tan\theta\right] \qquad (8.1.7.9)$$

and $L$ is the Lorentz factor, $1/\left(\sin^2 2\theta - \zeta^2\right)^{1/2}$.

The Guinier setting of an instrument (curved crystal monochromator case, Fig. 8.1.7.1*b*) gives $(\delta\lambda/\lambda)_{\text{corr}} = 0$. The equation for $\varphi_R$ then reduces to

$$\varphi_R = L\left[\left(\zeta^2\gamma_H^2 + \gamma_V^2/L^2\right)^{1/2} 2\varepsilon_s\right] \qquad (8.1.7.10)$$

(from Greenhough & Helliwell, 1982). For example, for $\zeta = 0$, $\gamma_V = 0.2$ mrad $(0.01^\circ)$, $\theta = 15^\circ$, $(\delta\lambda/\lambda)_{\text{conv}} = 1 \times 10^{-3}$ and $\eta = 0.8$ mrad $(0.05^\circ)$, then $\varphi_R = 0.08^\circ$. But $\varphi_R$ increases as $\zeta$ increases [see Greenhough & Helliwell (1982), Table 5]. In the rotation/oscillation method as applied to protein and virus crystals, a small angular range is used per exposure. For example, the maximum rotation range per image, $\Delta\varphi_{\text{max}}$, may be $1.5^\circ$ for a protein and

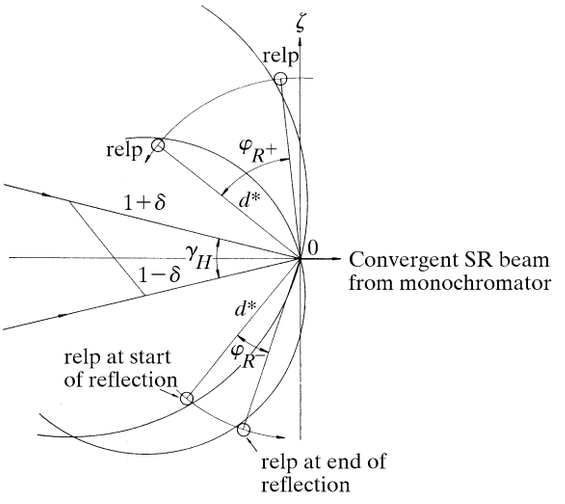


**Figure 8.1.7.3**
The rocking width of an individual reflection for the case of Fig. 8.1.7.1(*c*) and a vertical rotation axis. From Greenhough & Helliwell (1982).

$0.4^\circ$ or so for a virus. Many reflections will be only partially stimulated over the exposure. It is important, especially in the virus case, to predict the degree of penetration of the relp through the Ewald sphere. This is done by analysing the interaction of a spherical volume for a given relp with the Ewald sphere. The radius of this volume is given by

$$E \simeq \varphi_R/2L \qquad (8.1.7.11)$$

(Greenhough & Helliwell, 1982).

In Fig. 8.1.7.3, the relevant parameters are shown. The diagram shows $(\delta\lambda/\lambda)_{\text{corr}} = 2\delta$ in a plane, usually horizontal with a perpendicular (vertical) rotation axis, whereas the formula for $\varphi_R$ above is for a horizontal axis. This is purely for didactic reasons since the interrelationship of the components is then much clearer.

The limits of protein-crystal rocking widths have been explored by Helliwell (1988), Colapietro *et al.* (1992) and Snell (1995), whereby arc-second crystal precision has been observed at room temperature, *i.e.* unfrozen protein crystals. Special analysis software (Lovelace *et al.*, 2000) has been written to extract such precise crystal mosaicity values and the experiment obviously requires stringent (usually undulator) collimation. Exact comparisons of mosaicity values need reflection indexing, *e.g.* see Snell *et al.* (1995).

### 8.1.8. Scientific utilization of SR in protein crystallography

There are a myriad of applications and results of the use of SR in crystallography. Helliwell (1992) gave an extensive survey and tabulations of SR and macromolecular crystallography applications; Chapter 9 therein concentrates on anomalous scattering and Chapter 10 on high resolution, large unit cells, small crystals, weak scattering efficiency and time-resolved data collection. The field has expanded so dramatically, in fact, that an equivalent survey today would be vast. Table 8.1.4.1 lists the web pages of the facilities, where the specifications and details of the beamlines can be found (*e.g.* all the publications at Daresbury in the protein crystallography area organized by beamline instrument are to be found at http://dlwebres.dl.ac.uk/dl_public/publications/index.jsp). The examples below cite extreme cases of the large unit cell (virus and multi-macromolecular) cases, weak anomalous-scattering signal in MAD, fast time-resolved Laue

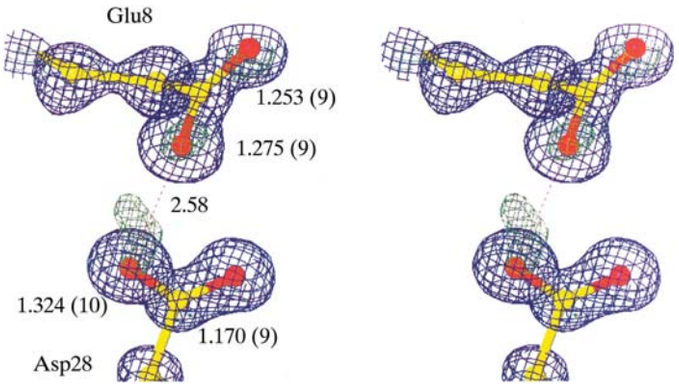


**Figure 8.1.8.1**
Determination of the protonation states of carboxylic acid side chains in proteins *via* hydrogen atoms and resolved single and double bond lengths. After Deacon *et al.* (1997) using CHESS. Reproduced by permission of The Royal Society of Chemistry.

studies and the ultra-high-resolution and even valence-density structure determinations to date. Another phasing technique involving multiple ('*n*-beam') diffraction is also being applied to proteins [Weckert & Hümmer (1997) at the ESRF and the NSLS]. These examples at least indicate the present bounds of capability of the various sub-fields of SR and macromolecular crystallography.

### *8.1.8.1. Atomic and ultra-high-resolution macromolecular crystallography*

The use of high SR intensity, cryo-freezing of a protein crystal to largely overcome radiation damage and sensitive, automatic area detectors (CCDs and/or image plates) is allowing diffraction data to be recorded at resolutions equivalent to smaller-molecule (chemical) crystallography. In a growing number of protein crystal structure studies, atomic resolution (1.2 Å or better) is achievable (Dauter *et al.*, 1997). The 'X-ray data to parameter' ratio can be favourable enough for single and double bonds, *e.g.* in carboxyl side chains, to be resolved [Fig. 8.1.8.1; Deacon *et al.* (1997) for concanavalin A at 0.94 Å resolution]. Along with this bond-distance precision, one can see the reactive proton directly. This approach complements H/D exchange neutron diffraction studies. Neutron studies have expanded in scope by employing Laue geometry in a synergistic development with SR Laue diffraction (Helliwell & Wilkinson, 1994; Helliwell, 1997*b*; Habash *et al.*, 1997, 2000); a comprehensive survey of neutron macromolecular crystallography, instruments and results in determining the atomic details of protonation and hydration has been given by Blakeley (2009). In particularly well ordered protein structure cases, valence-electron-density descriptions are possible for those atoms with *B* factors ~<3 $Å^2$ [see *e.g.* Guillot *et al.* (2008) and Luger (2007)]. The scope and accuracy of protein crystal structures has been transformed. A diffraction-component precision index for characterizing the overall precision of protein structures has been given by Cruickshank (1999) and cast in terms of experimental parameters by Blow (2002).

### *8.1.8.2. Small crystals*

Compensating for small crystal sample volume by increasing the intensity at the sample has been of major interest from the outset, and tests showed that the use of ~20 μm-sized samples is feasible (Hedman *et al.*, 1985). Third-generation high spectral brightness sources were optimized for this application *via* micron-sized focal spot beams, as described in the *ESRF Foundation Phase Report* (1987). Applications of the ESRF microfocus beamline diffractometer (Perrakis *et al.*, 1999) include as an example the determination of the structure of the bacteriorhodopsin crystal at high resolution from micro-crystals (Pebay-Peyroula *et al.*, 1997). Experiments using extremely thin plates involving only 1000 protein molecular layers are described by Mayans & Wilmanns (1999) on the BW7B wiggler beamline at DESY, Hamburg. A variety of small crystals and SR, including tabulated sample scattering efficiencies, can be found in Helliwell (1992), pp. 410–414 and more recently in Riekel *et al.* (2005). The ESRF Upgrade (Fig 8.1.2.2) will push this into the sub-micron territory.

### *8.1.8.3. Time-resolved macromolecular crystallography*

Time-resolved SR Laue diffraction of light-sensitive proteins, such as CO Mb studied with sub-nanosecond time resolution in pump–probe experiments (see Srajer *et al.*, 1996), have shown direct structural changes as a function of time. Enzymes, likewise, are being studied directly by time-resolved methods *via* a variety of reaction initiation methods, including pH jump, substrate diffusion and light flash of caged compounds pre-equilibrated in the crystal. Flash freezing is increasingly used to trap molecular structures at optimal times in a reaction determined either by microspectrophotometry or repeated Laue 'flash photography'. Enzyme reaction rates can be altered through site-directed mutagenesis (*e.g.* see Niemann *et al.*, 1994; Helliwell *et al.*, 1998) and matched to diffraction-data acquisition times. For overviews, see the books edited by Cruickshank *et al.* (1992) and Helliwell & Rentzepis (1997), the recent review by Bourgeois & Weik (2009) and the companion chapter by Moffat (Chapter 8.2 in this volume).

### *8.1.8.4. Multi-macromolecular complexes*

There is now a wealth of results in this field and the reader must be referred to books such as Liljas *et al.* (2009) for a detailed exposition. Multi-macromolecular complexes, such as viruses (Rossmann *et al.*, 1985; Acharya *et al.*, 1989; Liddington *et al.*, 1991) (Fig. 8.1.8.2), the nucleosome (Luger *et al.*, 1997), light-harvesting complex (McDermott *et al.*, 1995) and the 13-subunit membrane-bound protein cytochrome *c* oxidase (Tsukihara *et al.*, 1996), and large-scale molecular assemblies like muscle (Holmes, 1998) are very firmly recognizable as biological entities whose crystal structure determinations relied on SR. These single-crystal structure determinations involved extremely large unit cells and became tractable despite very weak scattering strength. The crystals often showed extreme sensitivity to radiation (hundreds, even a thousand, crystals have been used to constitute a single data set). Cryocrystallography radiation protection is now used extensively in crystallographic data collection and was critical for work with ribosome crystals (Hope *et al.*, 1989); SR has been essential for these structure determinations (see *e.g.* Yonath, 1992; Yonath *et al.*, 1998; Ban *et al.*, 1998; Wimberley *et al.*, 2000; Noller, 2005). A very large multi-protein complex solved using data from the Daresbury SRS wiggler is the $F_1$ ATPase structure (Fig. 8.1.8.3), for which a share in the Nobel Prize for Chemistry in 1997 was awarded to John Walker in Cambridge. The structure (Abrahams *et al.*, 1994; Abrahams & Leslie, 1996) and the amino-acid sequence data, along with fluorescence microscopy, show how biochemical energy is harnessed to drive the proton pump across biological membranes, thus corroborating hypotheses about this process made over many years. This

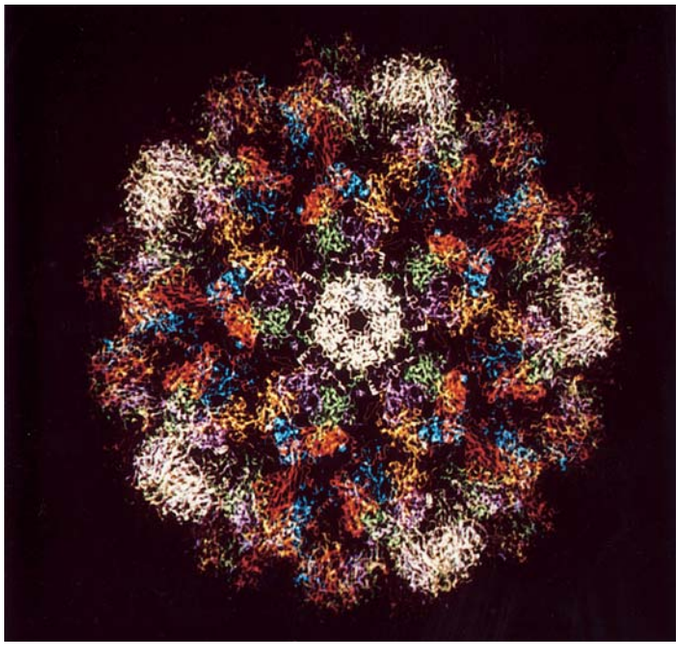

**Figure 8.1.8.2**
A view of SV40 virus (based on Liddington *et al.*, 1991) determined using data recorded at the SRS wiggler station 9.6 (Fig. 8.1.4.1*a*).

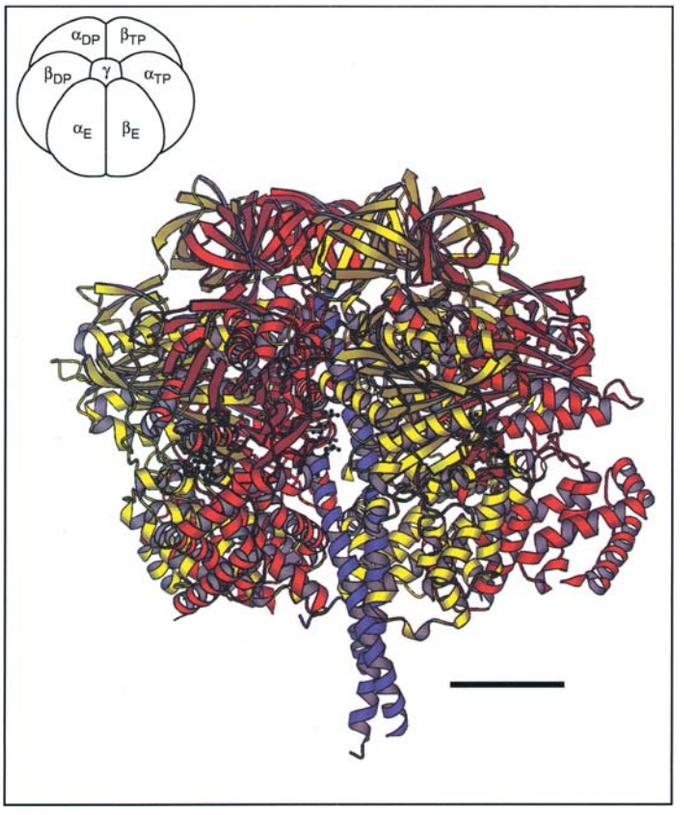


**Figure 8.1.8.3**
The protein crystal structure of $F_1$ ATPase, one of the largest non-symmetrical protein structure complexes, solved using SR data recorded on an image plate at the SRS wiggler 9.6, Daresbury. The scale bar is 20 Å long. Reprinted with permission from *Nature* (Abrahams *et al.*, 1994). Copyright (1994) MacMillan Magazines Limited.

study, made tractable by the SRS wiggler high-intensity protein crystallography station (Fig. 8.1.4.1), illustrates the considerable further scope that became possible with third-generation SR sources, such as the 780 Å diameter blue tongue virus (Grimes *et al.*, 1997, 1998) and the nucleosome core particle (Luger *et al.*, 1997). Spectacular progress has been made in the structural biology of photosynthesis using SR sources, which is not only yielding answers on this vital natural process but also stimulating much research to help address artificial energy sources based on this natural system. This research could have profound climate-change impacts with 'greener energy sources'. One such structure is the Photosystem II (PSII; see Fig. 8.1.8.4). This topic has been reviewed recently by Barber (2009); the atomic details of the $Mn_4Ca$ cluster of PSII have proved to be especially challenging to X-ray study (Yano *et al.*, 2005). These large-scale molecular assemblies often combine electron-microscope and diffraction techniques with SR X-ray crystallography and diffraction for low-to-high resolution detail, respectively.

### *8.1.8.5. Optimized anomalous dispersion (MAD), improved multiple isomorphous replacement (MIR) data and 'structural genomics'*

Rapid protein structure determination *via* the MAD method, notably involving seleno protein variants (Hendrickson *et al.*, 1990) as well as xenon pressure derivatives (see *e.g.* Schiltz *et al.*, 1997; Cianci *et al.*, 2001), and improved heavy-atom isomorphous replacement data are removing a major bottleneck in protein crystallography: that of phase determination. Databases of successful heavy-atom compounds (see *e.g.* Sugahara *et al.*, 2009) have been compiled and are increasingly sophisticated. Overall, as the number of protein structures in the Protein Data Bank doubles every few years, the possibility of considering whole genome-level structure determinations arises (Chayen *et al.*, 1996; Chayen & Helliwell, 1998). The human genome comprises some 35 000 genes. Of these, some 40% are coding for membrane-bound proteins, which are more difficult to crystallize. Since a MAD protein crystal structure currently requires less than 1 day of SR BM beamtime, the new 'bottlenecks' are protein production and crystallization. Thus, structural genomics projects have established 'pipelines' for protein structure determination with a view to creating a complete 'protein folds space'. This approach, along with homology modelling and genetic alignment techniques, opens the immense potential for structural genomics to yield huge numbers of experimentally derived protein structures and thereby a much better basis for understanding and controlling disease through structure-based drug design and

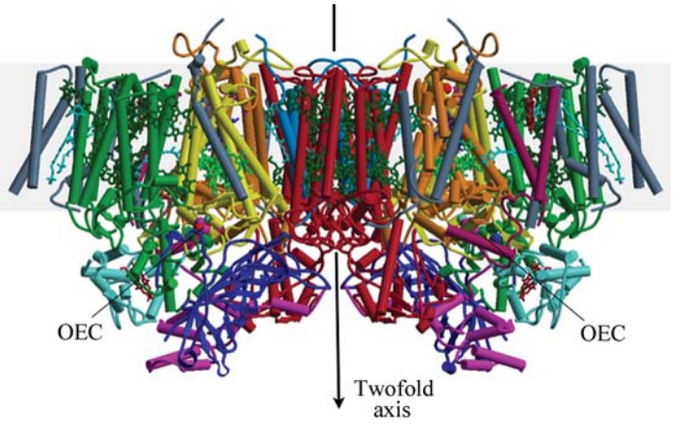


**Figure 8.1.8.4**
Side view of the structure of Photosystem II, the water-splitting enzyme of photosynthesis, determined using X-ray crystallography based on data recorded at the SLS and ESRF (Ferreira *et al.*, 2004). Kindly provided by Professor So Iwata, Imperial College, London.

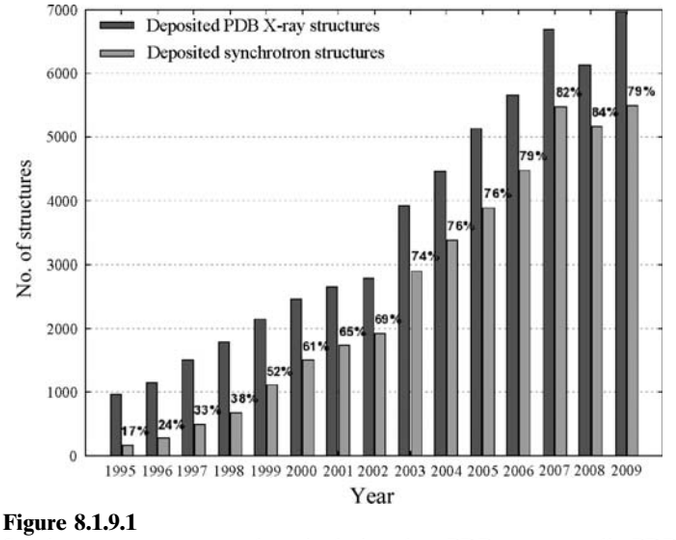


**Figure 8.1.9.1**
Synchrotron structures deposited in the PDB *versus* all PDB deposited structures (from http://biosync.rcsb.org/BiosyncStat.html) as of December 2009, *i.e.* a majority of all determined macromolecular crystal structures are now synchrotron-radiation derived.

discovery [for an early description see Bugg *et al.* (1993), for an example of pharmaceutical company collaboration see the Industrial Macromolecular Crystallography Association (IMCA) Collaborative Access Team at APS in Chicago (http://www.imca.aps.anl.gov/) and for a recent European perspective see *e.g.* Maclean *et al.* (2006).]

*8.1.8.6. Radiation damage*

The successes of these sources in macromolecular crystallography have been spectacular, so much so that provision of such beamlines now accounts for ~40% of the APS and ESRF insertion-device sectors. Nevertheless, X-radiation damage has been a continuing concern not least as the 'cutting edge' of capability to study ever-smaller crystals and ever-larger unit cells at synchrotron-radiation sources has been improved and optimized. A notable development has been a series of International Workshops on X-ray Damage to Crystalline Biological Samples. Most of these workshops have resulted in special issues of the *Journal of Synchrotron Radiation* (Volume 9 part 6, Volume 12 part 3, Volume 14 part 1 and Volume 16 part 2). The latest of these has a mini-review by Garman & Nave (2009).

### 8.1.9. Concluding remarks

SR and crystallography are now intricately intertwined in their scientific futures and in facilities provision (see *e.g.* Helliwell, 1998; Dauter, 2006; Fig. 8.1.9.1). Jiang & Sweet (2004) have given a systematic analysis of the impact of SR on macromolecular crystallography capabilities.

The new XFELs have produced very novel possibilities for 3D structure determination not only of non-crystallizable proteins but also whole cells (Neutze *et al.*, 2000; Miao *et al.*, 2001; Sayre, 2008; Shapiro, 2008). Whilst these approaches have attracted controversy, they represent a bold new push of X-ray diffraction methods towards widening capabilities in important frontiers in structural biology and structural cellular biology.

### References


Abrahams, J. P. & Leslie, A. G. W. (1996). *Methods used in the structure determination of bovine mitochondrial $F_1$ ATPase. Acta Cryst.* D**52**, 30–42.

Abrahams, J. P., Leslie, A. G. W., Lutter, R. & Walker, J. E. (1994). *Structure at 2.8 Å resolution of F1-ATPase from bovine heart mitochondria. Nature (London)*, **370**, 621–628.

Acharya, R., Fry, E., Stuart, D., Fox, G., Rowlands, D. & Brown, F. (1989). *The 3-dimensional structure of foot and mouth disease virus at 2.9 Å resolution. Nature (London)*, **337**, 709–716.

Allinson, N. M. (1994). *Development of non-intensified charge-coupled device area X-ray detectors. J. Synchrotron Rad.* **1**, 54–62.

Amemiya, Y. (1997). *X-ray storage phosphor imaging plate detectors: high sensitivity X-ray area detector. Methods Enzymol.* **276**, 233–243.

Andrews, S. J., Hails, J. E., Harding, M. M. & Cruickshank, D. W. J. (1987). *The mosaic spread of very small crystals deduced from Laue diffraction patterns. Acta Cryst.* A**43**, 70–73.

Arndt, U. W., Greenhough, T. J., Helliwell, J. R., Howard, J. A. K., Rule, S. A. & Thompson, A. W. (1982). *Optimised anomalous dispersion crystallography: a synchrotron X-ray polychromatic simultaneous profile method. Nature (London)*, **298**, 835–838.

Arnold, E., Vriend, G., Luo, M., Griffith, J. P., Kamer, G., Erickson, J. W., Johnson, J. E. & Rossmann, M. G. (1987). *The structure determination of a common cold virus, human rhinovirus 14. Acta Cryst.* A**43**, 346–361.

Arzt, S., Campbell, J. W., Harding, M. M., Hao, Q. & Helliwell, J. R. (1999). *LSCALE – the new normalization, scaling and absorption correction program in the Daresbury Laue software suite. J. Appl. Cryst.* **32**, 554–562.

Baker, P. J., Farrants, G. W., Stillman, T. J., Britton, K. L., Helliwell, J. R. & Rice, D. W. (1990). *Isomorphous replacement with optimized anomalous scattering applied to protein crystallography. Acta Cryst.* A**46**, 721–725.

Ban, N., Freeborn, B., Nissen, P., Penczek, P., Grassucci, R. A., Sweet, R., Frank, J., Moore, P. B. & Steitz, T. A. (1998). *A 9 Å resolution X-ray crystallographic map of the large ribosomal subunit. Cell*, **93**, 1105–1115.

Barber, J. (2009). *Photosynthetic energy conversion: natural and artificial. Chem. Soc. Rev.* **38**, 185–196.

Bartunik, H. D., Clout, P. N. & Robrahn, B. (1981). *Rotation data collection for protein crystallography with time-variable incident intensity from synchrotron radiation sources. J. Appl. Cryst.* **14**, 134–136.

Beuville, E., Beche, J. F., Cork, C., Douence, V., Earnest, T., Millaud, J., Nygren, D., Padmore, H., Turko, B., Zizka, G., Datte, P. & Xuong, N. H. (1997). *A 16 × 16 pixel array detector for protein crystallography. Nucl. Instrum. Methods*, **395**, 429–434.

Bilderback, D. H. (1986). *The potential of cryogenic silicon and germanium X-ray monochromators for use with large synchrotron heat loads. Nucl. Instrum. Methods*, **246**, 434–436.

Blakeley, M. P. (2009). *Neutron macromolecular crystallography. Crystallogr. Rev.* **15**, 157–218.

Blewett, J. P. (1946). *Radiation losses in the induction electron accelerator. Phys. Rev.* **69**, 87–95.

Blow, D. M. (2002). *Rearrangement of Cruickshank's formulae for the diffraction-component precision index. Acta Cryst.* D**58**, 792–797.

Bonse, U., Materlik, G. & Schröder, W. (1976). *Perfect-crystal monochromators for synchrotron X-radiation. J. Appl. Cryst.* **9**, 223–230.

Bourenkov, G. P., Popov, A. N. & Bartunik, H. D. (1996). *A Bayesian approach to Laue diffraction analysis and its potential for time-resolved protein crystallography. Acta Cryst.* A**52**, 797–811.

Bourgeois, D. & Weik, M. (2009). *Kinetic protein crystallography: a tool to watch proteins in action. Crystallogr. Rev.* **15**, 87–118.

Brammer, R., Helliwell, J. R., Lamb, W., Liljas, A., Moore, P. R., Thompson, A. W. & Rathbone, K. (1988). *A new protein crystallography station on the SRS wiggler beamline for very rapid Laue and rapidly tunable monochromatic experiments: I. Design principles, ray tracing and heat calculations. Nucl. Instrum. Methods A*, **271**, 678–687.

Branden, C. I. (1994). *The new generation of synchrotron machines. Structure*, **2**, 5–6.

Brinkmann, R., Materlik, G., Rossbach, J., Schneider, J. R. & Wilk, B. H. (1997). *An X-ray FEL laboratory as part of a linear collider design. Nucl. Instrum. Methods*, **393**, No. 1–3, 86–92.

Broennimann, Ch., Eikenberry, E. F., Henrich, B., Horisberger, R., Huelsen, G., Pohl, E., Schmitt, B., Schulze-Briese, C., Suzuki, M., Tomizaki, T., Toyokawa, H. & Wagner, A. (2006). *The PILATUS 1M detector J. Synchrotron Rad.* **13**, 120–130.

Bugg, C. E., Carson, W. M. & Montgomery, J. A. (1993). *Drugs by design. Sci. Am.* **269**, 60–66.

Campbell, J. W. & Hao, Q. (1993). *Evaluation of reflection intensities for the components of multiple Laue diffraction spots. II. Using the wavelength-normalization curve. Acta Cryst.* A**49**, 889–893.

Caspar, D. L. D., Clarage, J., Salunke, D. M. & Clarage, M. (1988). *Liquid-like movements in crystalline insulin. Nature (London)*, **352**, 659–662.

Cassetta, A., Deacon, A., Emmerich, C., Habash, J., Helliwell, J. R., McSweeney, S., Snell, E., Thompson, A. W. & Weisgerber, S. (1993). *The emergence of the synchrotron Laue method for rapid data collection from protein crystals. Proc. R. Soc. London Ser. A*, **442**, 177–192.

Cauchois, Y., Bonnelle, C. & Missoui, G. (1963). *Rayonnement electromagnetique – premiers spectres X du rayonnement d'orbite du synchrotron de Frascati. C. R. Acad. Sci. Paris*, **257**, 409–412.

Charpak, G. (1970). *Evolution of the automatic spark chambers. Annu. Rev. Nucl. Sci.* **20**, 195–254.

Chayen, N. E., Boggon, T. J., Cassetta, A., Deacon, A., Gleichmann, T., Habash, J., Harrop, S. J., Helliwell, J. R., Nieh, Y. P., Peterson, M. R., Raftery, J., Snell, E. H., Hädener, A., Niemann, A. C., Siddons, D. P., Stojanoff, V., Thompson, A. W., Ursby, T. & Wulff, M. (1996). *Trends and challenges in experimental macromolecular crystallography. Q. Rev. Biophys.* **29**, 227–278.

Chayen, N. E. & Helliwell, J. R. (1998). *Protein crystallography: the human genome in 3-D. Phys. World*, **11**, No. 5, 43–48.

Cianci, M., Antonyuk, S., Bliss, N., Bailey, M. W., Buffey, S. G., Cheung, K. C., Clarke, J. A., Derbyshire, G. E., Ellis, M. J., Enderby, M. J., Grant, A. F., Holbourn, M. P., Laundy, D., Nave, C., Ryder, R., Stephenson, P., Helliwell, J. R. & Hasnain, S. S. (2005). *A high-throughput structural biology/proteomics beamline at the SRS on a new multipole wiggler. J. Synchrotron Rad.* **12**, 455–466.

Cianci, M., Helliwell, J. R. & Suzuki, A. (2008). *The interdependence of wavelength, redundancy and dose in sulfur SAD experiments. Acta Cryst.* D**64**, 1196–1209.

Cianci, M., Rizkallah, P. J., Olczak, A., Raftery, J., Chayen, N. E., Zagalsky, P. F. & Helliwell, J. R. (2001). *Structure of lobster apocrustacyanin $A_1$ using softer X-rays. Acta Cryst.* D**57**, 1219–1229.

Colapietro, M., Cappuccio, G., Marciante, C., Pifferi, A., Spagna, R. & Helliwell, J. R. (1992). *The X-ray diffraction station at the ADONE wiggler facility: preliminary results (including crystal perfection). J. Appl. Cryst.* **25**, 192–194.

Cruickshank, D. W. J. (1999). *Remarks about protein structure precision. Acta Cryst.* D**55**, 583–601.

Cruickshank, D. W. J., Helliwell, J. R. & Johnson, L. N. (1992). Editors. *Time-resolved Macromolecular Crystallography.* Oxford: OUP/The Royal Society.

Cruickshank, D. W. J., Helliwell, J. R. & Moffat, K. (1987). *Multiplicity distribution of reflections in Laue diffraction. Acta Cryst.* A**43**, 656–674.

Cruickshank, D. W. J., Helliwell, J. R. & Moffat, K. (1991). *Angular distribution of reflections in Laue diffraction. Acta Cryst.* A**47**, 352–373.

Dauter, Z. (2006). *Current state and prospects of macromolecular crystallography. Acta Cryst.* (2006). D**62**, 1–11.

Dauter, Z., Lamzin, V. S. & Wilson, K. S. (1997). *The benefits of atomic resolution. Curr. Opin. Struct. Biol.* **7**, 681–688.

Deacon, A., Gleichmann, T., Kalb (Gilboa), A. J., Price, H., Raftery, J., Bradbrook, G., Yariv, J. & Helliwell, J. R. (1997). *The structure of concanavalin A and its bound solvent determined with small-molecule accuracy at 0.94 Å resolution. J. Chem. Soc. Faraday Trans.* **93**, 4305–4312.

Doniach, S., Hodgson, K., Lindau, I., Pianetta, P. & Winick, H. (1997). *Early work with synchrotron radiation at Stanford. J. Synchrotron Rad.* **4**, 380–395.

Doucet, J. & Benoit, J. P. (1987). *Molecular dynamics by analysis of the X-ray diffuse scattering from lysozyme crystals. Nature (London)*, **325**, 643–646.

Dumas, C., Duquerroy, S. & Janin, J. (1995). *Phasing with mercury at 1 Å wavelength. Acta Cryst.* D**51**, 814–818.

Eikenberry, E. F., Barna, S. L., Tate, M. W., Rossi, G., Wixted, R. L., Sellin, P. J. & Gruner, S. M. (1998). *A pixel-array detector for time-resolved X-ray diffraction. J. Synchrotron. Rad.* **5**, 252–255.

Einspahr, H., Suguna, K., Suddath, F. L., Ellis, G., Helliwell, J. R. & Papiz, M. Z. (1985). *The location of manganese and calcium ion cofactors in pea lectin crystals by use of anomalous dispersion and tuneable synchrotron X-radiation. Acta Cryst.* B**41**, 336–341.

Elleaume, P. (1989). *Special synchrotron radiation sources. Part 1: conventional insertion devices. Synchrotron Radiat. News*, **1**, 18–23.

Elleaume, P. (1998). *Two-plane focusing of 30 keV undulator radiation. J. Synchrotron Rad.* **5**, 1–5.

*ESRF Foundation Phase Report* (1987). Grenoble: ESRF.

Ferreira, K. N., Iverson, T. M., Maghlaoui, K., Barber, J. & Iwata, S. (2004). *Architecture of the photosynthetic oxygen-evolving center. Science*, **303**, 1831–1838.

Fourme, R. (1997). *Position-sensitive gas detectors: MWPCs and their gifted descendants. Nucl. Instrum. Methods A*, **392**, 1–11.

Fourme, R., Kahn, R., Mezouar, M., Girard, E., Hoerentrup, C., Prangé, T. & Ascone, I. (2001). *High-pressure protein crystallography (HPPX): instrumentation, methodology and results on lysozyme crystals. J. Synchrotron Rad.* **8**, 1149–1156.

Freund, A. K. (1996). *Third-generation synchrotron radiation X-ray optics. Structure*, **4**, 121–125.

Garman, E. F. & Nave, C. (2009). *Radiation damage in protein crystals examined under various conditions by different methods J. Synchrotron Rad.* **16**, 129–132.

Girard, E., Dhaussy, A.-C., Couzinet, B., Chervin, J.-C., Mezouar, M., Kahn, R., Ascone, I. & Fourme, R. (2007). *Toward fully fledged high-pressure macromolecular crystallography. J. Appl. Cryst.* **40**, 912–918.

Glover, I. D., Harris, G. W., Helliwell, J. R. & Moss, D. S. (1991). *The variety of X-ray diffuse scattering from macromolecular crystals and its respective components. Acta Cryst.* B**47**, 960–968.

Gonzalez, A., Cohen, A., Eriksson, T., McPhillips, S., Moorhead, P., Narevicius, J., Sharp, K., Smith, C., Song, J. & Soltis, S. M. (2005). *Facility updates: remote access to the SSRL macromolecular crystallography beamlines. Synchrotron Radiat. News*, **18**, 36–39.

Greenhough, T. J. & Helliwell, J. R. (1982). *Oscillation camera data processing: reflecting range and prediction of partiality. II. Monochromatised synchrotron X-radiation from a singly bent triangular monochromator. J. Appl. Cryst.* **15**, 493–508.

Grimes, J. M., Burroughs, J. N., Gouet, P., Diprose, J. M., Malby, R., Zientara, S., Mertens, P. P. C. & Stuart, D. I. (1998). *The atomic structure of the bluetongue virus core. Nature (London)*, **395**, 470–478.

Grimes, J. M., Jakana, J., Ghosh, M., Basak, A. K., Roy, P., Chiu, W., Stuart, D. I. & Prasad, B. V. V. (1997). *An atomic model of the outer layer of the bluetongue virus core derived from X-ray crystallography and electron cryomicroscopy. Structure*, **5**, 885–893.

Gruner, S. M. & Ealick, S. E. (1995). *Charge coupled device X-ray detectors for macromolecular crystallography. Structure*, **3**, 13–15.

Guillot, B., Jelsch, C., Podjarny, A. & Lecomte, C. (2008). *Charge-density analysis of a protein structure at subatomic resolution: the human aldose reductase case. Acta Cryst.* D**64**, 567–588.

Guss, J. M., Merritt, E. A., Phizackerley, R. P., Hedman, B., Murata, M., Hodgson, K. O. & Freeman, H. C. (1988). *Phase determination by multiple wavelength X-ray diffraction – crystal structure of a basic blue copper protein from cucumbers. Science*, **241**, 806–811.

Habash, J., Raftery, J., Nuttall, R., Price, H. J., Wilkinson, C., Kalb (Gilboa), A. J. & Helliwell, J. R. (2000). *Direct determination of the positions of the deuterium atoms of the bound water in concanavalin A by neutron Laue crystallography. Acta Cryst.* D**56**, 541–550.

Habash, J., Raftery, J., Weisgerber, S., Cassetta, A., Lehmann, M. S., Hoghoj, P., Wilkinson, C., Campbell, J. W. & Helliwell, J. R. (1997). *Neutron Laue diffraction study of concanavalin A: the proton of Asp28. J. Chem. Soc. Faraday Trans.* **93**, 4313–4317.

Hädener, A., Matzinger, P. K., Battersby, A. R., McSweeney, S., Thompson, A. W., Hammersley, A. P., Harrop, S. J., Cassetta, A., Deacon, A., Hunter, W. N., Nieh, Y. P., Raftery, J., Hunter, N. & Helliwell, J. R. (1999). *Determination of the structure of selenomethionine-labelled hydroxymethylbilane synthase in its active form by multi-wavelength anomalous dispersion. Acta Cryst.* D**55**, 631–643.

Hajdu, J., Acharya, K. R., Stuart, D. I., McLaughlin, P. J., Barford, D., Oikonomakos, N. G., Klein, H. & Johnson, L. N. (1987). *Catalysis in the crystal – synchrotron radiation studies with glycogen phosphorylase. EMBO J.* **6**, 539–546.

Hajdu, J., Machin, P. A., Campbell, J. W., Greenhough, T. J., Clifton, I. J., Zurek, S., Gover, S., Johnson, L. N. & Elder, M. (1987). *Millisecond X-ray diffraction and the first electron density map from Laue photographs of a protein crystal. Nature (London)*, **329**, 178–181.

Hall, G. (1995). *Silicon pixel detectors for X-ray diffraction studies at synchrotron sources. Q. Rev. Biophys.* **28**, 1–32.

Harmsen, A., Leberman, R. & Schultz, G. E. (1976). *Comparison of protein crystal diffraction patterns and absolute intensities from synchrotron and conventional X-ray sources. J. Mol. Biol.* **104**, 311–314.

Hart, M. (1971). *Bragg reflection X-ray optics. Rep. Prog. Phys.* **34**, 435–490.

Haslegrove, J. C., Faruqi, A. R., Huxley, H. E. & Arndt, U. W. (1977). *The design and use of a camera for low-angle X-ray diffraction experiments with synchrotron radiation. J. Phys. E*, **10**, 1035–1044.

Hastings, J. B. (1977). *X-ray optics and monochromators for synchrotron radiation. J. Appl. Phys.* **48**, 1576–1584.

Hastings, J. B., Kincaid, B. M. & Eisenberger, P. (1978). *A separated function focusing monochromator system for synchrotron radiation. Nucl. Instrum. Methods*, **152**, 167–171.

Hedman, B., Hodgson, K. O., Helliwell, J. R., Liddington, R. & Papiz, M. Z. (1985). *Protein micro-crystal diffraction and the effects of radiation damage with ultra high flux synchrotron radiation. Proc. Natl Acad. Sci. USA*, **82**, 7604–7607.

Helliwell, J. R. (1977). *Application of synchrotron radiation to protein crystallography: preliminary experiments on 6PDGH crystals using the NINA synchrotron, Daresbury, UK.* DPhil thesis, University of Oxford, Appendix 1.

Helliwell, J. R. (1979). *Optimisation of anomalous scattering and structural studies of proteins using synchrotron radiation.* In *Proceedings of the Study Weekend. Applications of SR to the Study of Large Molecules of Chemical and Biological Interest*, edited by R. B. Cundall & I. H. Munro, pp. 1–6. DL/SCI/R13. Warrington: Daresbury Laboratory.

Helliwell, J. R. (1984). *Synchrotron X-radiation protein crystallography: instrumentation, methods and applications. Rep. Prog. Phys.* **47**, 1403–1497.

Helliwell, J. R. (1985). *Protein crystallography with synchrotron radiation. J. Mol. Struct.* **130**, 63–91.

Helliwell, J. R. (1988). *Protein crystal perfection and the nature of radiation damage*. *J. Crystal Growth*, **90**, 259–272.

Helliwell, J. R. (1992). *Macromolecular Crystallography with Synchrotron Radiation.* Cambridge University Press.

Helliwell, J. R. (1993). *The choice of X-ray wavelength in macromolecular crystallography*. In *Computational Aspects of Data Collection*, compiled by S. Bailey, pp. 80–88. DL/SCI/R34. Warrington: Daresbury Laboratory.

Helliwell, J. R. (1997*a*). *Overview on synchrotron radiation and application in macromolecular crystallography. Methods Enzymol.* **276**, 203–217.

Helliwell, J. R. (1997*b*). *Neutron Laue diffraction does it faster. Nature Struct. Biol.* **4**, 874–876.

Helliwell, J. R. (1998). *Synchrotron radiation and crystallography: the first fifty years. Acta Cryst.* A**54**, 738–749.

Helliwell, J. R. (2004). *Overview and new developments in softer X-ray (2 Å < λ< 5 Å) protein crystallography*. *J. Synchrotron Rad.* **11**, 1–3.

Helliwell, J. R., Ealick, S., Doing, P., Irving, T. & Szebenyi, M. (1993). *Towards the measurement of ideal data for macromolecular crystallography using synchrotron sources. Acta Cryst.* D**49**, 120–128.

Helliwell, J. R., Habash, J., Cruickshank, D. W. J., Harding, M. M., Greenhough, T. J., Campbell, J. W., Clifton, I. J., Elder, M., Machin, P. A., Papiz, M. Z. & Zurek, S. (1989). *The recording and analysis of synchrotron X-radiation Laue diffraction photographs. J. Appl. Cryst.* **22**, 483–497.

Helliwell, J. R., Nieh, Y. P., Raftery, J., Cassetta, A., Habash, J., Carr, P. D., Ursby, T., Wulff, M., Thompson, A. W., Niemann, A. C. & Hädener, A. (1998). *Time-resolved structures of hydroxymethylbilane synthase (Lys59Gln mutant) as it is loaded with substrate in the crystal determined by Laue diffraction. J. Chem. Soc. Faraday Trans.* **94**, 2615–2622.

Helliwell, J. R., Papiz, M. Z., Glover, I. D., Habash, J., Thompson, A. W., Moore, P. R., Harris, N., Croft, D. & Pantos, E. (1986). *The wiggler protein crystallography workstation at the Daresbury SRS; progress and results. Nucl. Instrum. Methods A*, **246**, 617–623.

Helliwell, J. R. & Rentzepis, P. M. (1997). Editors. *Time-resolved Diffraction.* Oxford University Press.

Helliwell, J. R. & Wilkinson, C. (1994). *X-ray and neutron Laue diffraction*. In *Neutron and Synchrotron Radiation for Condensed Matter Studies*, Vol. 3, edited by J. Baruchel, J. L. Hodeau, M. S. Lehmann, J. R. Regnard & C. Schlenker, ch. 12. Berlin: Springer Verlag.

Hendrickson, W. A. (1985). *Analysis of protein structure from diffraction measurements at multiple wavelengths. Trans. Am. Crystallogr. Assoc.* **21**, 11–21.

Hendrickson, W. A., Horton, J. R. & LeMaster, D. M. (1990). *Selenomethionyl proteins produced for analysis by multi-wavelength anomalous diffraction (MAD) – a vehicle for direct determination of 3-dimensional structure. EMBO J.* **9**, 1665–1672.

Hendrickson, W. A., Pahler, A., Smith, J. L., Satow, Y., Merritt, E. A. & Phizackerley, R. P. (1989). *Crystal structure of core streptavadin determined from multi-wavelength anomalous diffraction of synchrotron radiation. Proc. Natl Acad. Sci. USA*, **86**, 2190–2194.

Herzenberg, A. & Lau, H. S. M. (1967). *Anomalous scattering and the phase problem. Acta Cryst.* **22**, 24–28.

Holmes, K. C. (1998). *A molecular model for muscle contraction. Acta Cryst.* A**54**, 789–797.

Hope, H., Frolow, F., von Böhlen, K., Makowski, I., Kratky, C., Halfon, Y., Danz, H., Webster, P., Bartels, K. S., Wittmann, H. G. & Yonath, A. (1989). *Cryocrystallography of ribosomal particles. Acta Cryst.* B**45**, 190–199.

Hoppe, W. & Jakubowski, V. (1975). *The determination of phases of erythrocruorin using the two-wavelength method with iron as anomalous scatterer.* In *Anomalous Scattering*, edited by S. Ramaseshan & S. C. Abrahams, pp. 437–461. Copenhagen: Munksgaard.

Huxley, H. E. & Holmes, K. C. (1997). *Development of synchrotron radiation as a high-intensity source for X-ray diffraction. J. Synchrotron Rad.* **4**, 366–379.

Iwanenko, D. & Pomeranchuk, I. (1944). *On the maximal energy attainable in a betatron. Phys. Rev.* **65**, 343.

Jakoncic, J., Di Michiel, M., Zhong, Z., Honkimaki, V., Jouanneau, Y. & Stojanoff, V. (2006). *Anomalous diffraction at ultra-high energy for protein crystallography*. *J. Appl. Cryst.* **39**, 831–841.

Jiang, J. & Sweet, R. M. (2004). *Protein Data Bank depositions from synchrotron sources*. *J. Synchrotron Rad.* **11**, 319–327.

Kahn, R., Fourme, R., Bosshard, R., Chiadmi, M., Risler, J. L., Dideberg, O. & Wery, J. P. (1985). *Crystal structure study of opsanus-tau parvalbumin by multi-wavelength anomalous dispersion. FEBS Lett.* **170**, 133–137.

Karle, J. (1967). *Anomalous scatterers in X-ray diffraction and the use of several wavelengths. Appl. Opt.* **6**, 2132–2135.

Karle, J. (1980). *Some anomalous dispersion developments for the structure investigation of macromolecular systems in biology. Int. J. Quantum Chem. Symp.* **7**, 357–367.

Karle, J. (1989). *Macromolecular structure from anomalous dispersion. Phys. Today*, **42**, 22–29.

Karle, J. (1994). *Developments in anomalous scattering for structure determination.* In *Resonant Anomalous X-ray Scattering*, edited by G. Materlik, C. J. Sparks & K. Fischer, pp. 145–158. Amsterdam: North Holland.

Kohra, K., Ando, M., Matsushita, T. & Hashizume, H. (1978). *Design of high resolution X-ray optical system using dynamical diffraction for synchrotron radiation. Nucl. Instrum. Methods*, **152**, 161–166.

Korszun, Z. R. (1987). *The tertiary structure of azurin from pseudomonas-denitrificans as determined by Cu resonant diffraction using synchrotron radiation. J. Mol. Biol.* **196**, 413–419.

Lairson, B. M. & Bilderback, D. H. (1982). *Transmission X-ray mirror – a new optical element. Nucl. Instrum. Methods*, **195**, 79–83.

Lemonnier, M., Fourme, R., Rousseaux, F. & Kahn, R. (1978). *X-ray curved-crystal monochromator system at the storage ring DCI. Nucl. Instrum. Methods*, **152**, 173–177.

Lewis, R. (1994). *Multiwire gas proportional counters: decrepit antiques or classic performers? J. Synchrotron Rad.* **1**, 43–53.

Liddington, R. C., Yan, Y., Moulai, J., Sahli, R., Benjamin, T. L. & Harrison, S. C. (1991). *Structure of simian virus-40 at 3.8 Å resolution. Nature (London)*, **354**, 278–284.

Liljas, A., Liljas, L., Piskur, J., Lindblom, G., Nissen, P. & Kjeldgaard, M. (2009). *Textbook of Structural Biology*. Singapore: World Scientific.

Lindley, P. F. (1999). *Macromolecular crystallography with a third-generation synchrotron source. Acta Cryst.* D**55**, 1654–1662.

Liu, Y., Ogata, C. & Hendrickson, W. (2001). *Multiwavelength anomalous diffraction analysis at the M absorption edges of uranium*. *Proc. Natl Acad. Sci. USA*, **98**, 10648–10653.

Lovelace, J., Snell, E. H., Pokross, M., Arvai, A. S., Nielsen, C., Xuong, N.-H., Bellamy, H. D. & Borgstahl, G. E. O. (2000). *BEAM-ish: a graphical user interface for the physical characterization of macromolecular crystals*. *J. Appl. Cryst.* **33**, 1187–1188.

Luger, K., Mader, A. W., Richmond, R. K., Sargent, D. F. & Richmond, T. J. (1997). *Crystal structure of the nucleosome core particle at 2.8 Å resolution. Nature (London)*, **389**, 251–260.

Luger, P. (2007). *Fast electron density methods in the life sciences – a routine application in the future? Org. Biomol. Chem.* **5**, 2529–2540.
McDermott, G., Prince, S. M., Freer, A. A., Hawthornthwaite-Lawless, A. M., Papiz, M. Z., Cogdell, R. J. & Isaacs, N. W. (1995). *Crystal structure of an integral membrane light harvesting complex from photosynthetic bacteria. Nature (London)*, **374**, 517–521.
Maclean, E. J., Rizkallah, P. J. & Helliwell, J. R. (2006). *Protein crystallography and synchrotron radiation; current status and future landscape*. *Eur. Pharm. Rev.* **2**, 71–76.
Mayans, O. & Wilmanns, M. (1999). *X-ray analysis of protein crystals with thin-plate morphology. J. Synchrotron Rad.* **6**, 1016–1020.
Miao, J., Hodgson, K. O. & Sayre, D. (2001). *An approach to three-dimensional structures of biomolecules by using single-molecule diffraction images*. *Proc. Natl Acad. Sci. USA*, **98**, 6641–6645.
Miller, A. (1994). *Advanced Synchrotron Sources – Plans at ESRF in SR in Biophysics*, edited by S. S. Hasnain. Chichester: Ellis Horwood.
Mills, D. M., Helliwell, J. R., Kvick, Å., Ohta, T., Robinson, I. A. & Authier, A. (2005). *Report of the Working Group on Synchrotron Radiation Nomenclature – brightness, spectral brightness or brilliance? J. Synchrotron Rad.* **12**, 385.
Moffat, K., Szebenyi, D. & Bilderback, D. H. (1984). *X-ray Laue diffraction from protein crystals. Science*, **223**, 1423–1425.
Mukherjee, A. K., Helliwell, J. R. & Main, P. (1989). *The use of MULTAN to locate the positions of anomalous scatterers. Acta Cryst.* A**45**, 715–718.
Munro, I. H. (1997). *Synchrotron radiation research in the UK. J. Synchrotron Rad.* **4**, 344–358.
Neutze, R. & Hajdu, J. (1997). *Femtosecond time resolution in X-ray diffraction experiments. Proc. Natl Acad. Sci. USA*, **94**, 5651–5655.
Neutze, R., Wouts, R., Spoel, D., Weckert, E. & Hajdu, J. (2000). *Potential for biomolecular imaging with femtosecond X-ray pulses*. *Nature (London)*, **406**, 752–757.
Nieh, Y. P., Raftery, J., Weisgerber, S., Habash, J., Schotte, F., Ursby, T., Wulff, M., Hädener, A., Campbell, J. W., Hao, Q. & Helliwell, J. R. (1999). *Accurate and highly complete synchrotron protein crystal Laue diffraction data using the ESRF CCD and the Daresbury Laue software*. *J. Synchrotron Rad.* **6**, 995–1006.
Niemann, A. C., Matzinger, P. K. & Hadener, A. (1994). *A kinetic analysis of the reaction catalysed by hydroxymethylbilane synthase. Helv. Chim. Acta*, **77**, 1791–1809.
Noller, H. F. (2005). *RNA structure: reading the ribosome*. *Science*, **309**, 1508–1514.
Nugent, K. (2009). *Coherent methods in the X-ray sciences*. *Adv. Phys.* **59**, 1–99.
Okaya, Y. & Pepinsky, R. (1956). *New formulation and solution of the phase problem in X-ray analysis of non-centric crystals containing anomalous scatterers. Phys. Rev.* **103**, 1645–1647.
Parratt, L. G. (1959). *Use of synchrotron orbit-radiation in X-ray physics. Rev. Sci. Instrum.* **30**, 297–299.
Pebay-Peyroula, E., Rummel, G., Rosenbusch, J. P. & Landau, E. M. (1997). *X-ray structure of bacteriorhodopsin at 2.5 Å from micro-crystals grown in lipidic cubic phases. Science*, **277**, 1676–1681.
Perrakis, A., Cipriani, F., Castagna, J.-C., Claustre, L., Burghammer, M., Riekel, C. & Cusack, S. (1999). *Protein microcrystals and the design of a microdiffractometer: current experience and plans at EMBL and ESRF/ID13*. *Acta Cryst.* D**55**, 1765–1770.
Peterson, M. R., Harrop, S. J., McSweeney, S. M., Leonard, G. A., Thompson, A. W., Hunter, W. N. & Helliwell, J. R. (1996). *MAD phasing strategies explored with a brominated oligonucleotide crystal at 1.65 Å resolution. J. Synchrotron Rad.* **3**, 24–34.
Phillips, J. C. & Hodgson, K. O. (1980). *The use of anomalous scattering effects to phase diffraction patterns from macromolecules. Acta Cryst.* A**36**, 856–864.
Phillips, J. C., Templeton, L. K., Templeton, D. H. & Hodgson, K. O. (1978). *L-III edge anomalous X-ray scattering by cesium measured with synchrotron radiation. Science*, **201**, 257–259.
Phillips, J. C., Wlodawer, A., Goodfellow, J. M., Watenpaugh, K. D., Sieker, L. C., Jensen, L. H. & Hodgson, K. O. (1977). *Applications of synchrotron radiation to protein crystallography. II. Anomalous scattering, absolute intensity and polarization. Acta Cryst.* A**33**, 445–455.
Phillips, J. C., Wlodawer, A., Yevitz, M. M. & Hodgson, K. O. (1976). *Applications of synchrotron radiation to protein crystallography: preliminary results. Proc. Natl Acad. Sci. USA*, **73**, 128–132.
Polikarpov, I., Teplyakov, A. & Oliva, G. (1997). *The ultimate wavelength for protein crystallography? Acta Cryst.* D**53**, 734–737.
Ren, Z. & Moffat, K. (1995*a*). *Quantitative analysis of synchrotron Laue diffraction patterns in macromolecular crystallography. J. Appl. Cryst.* **28**, 461–481.
Ren, Z. & Moffat, K. (1995*b*). *Deconvolution of energy overlaps in Laue diffraction. J. Appl. Cryst.* **28**, 482–493.
Riekel, C. (2000). *New avenues in X-ray microbeam experiments*. *Rep. Prog. Phys.* **63**, 233–262.
Riekel, C., Burghammer, M. & Schertler, G. (2005). *Protein crystallography microdiffraction*. *Curr. Opin. Struct. Biol.* **15**, 556–562.
Rosenbaum, G., Holmes, K. C. & Witz, J. (1971). *Synchrotron radiation as a source for X-ray diffraction. Nature (London)*, **230**, 434–437.
Rossmann, M. G., Arnold, E., Erickson, J. W., Frankenberger, E. A., Griffith, J. P., Hecht, H. J., Johnson, J. E., Kamer, G., Luo, M., Mosser, A. G., Rueckert, R. R., Sherry, B. & Vriend, G. (1985). *Structure of a human common cold virus and functional relationship to other picornaviruses. Nature (London)*, **317**, 145–153.
Rossmann, M. G. & Erickson, J. W. (1983). *Oscillation photography of radiation-sensitive crystals using a synchrotron source. J. Appl. Cryst.* **16**, 629–636.
Sakabe, N. (1983). *A focusing Weissenberg camera with multi-layer-line screens for macromolecular crystallography. J. Appl. Cryst.* **16**, 542–547.
Sakabe, N. (1991). *X-ray diffraction data collection system for modern protein crystallography with a Weissenberg camera and an imaging plate using synchrotron radiation. Nucl. Instrum. Methods A*, **303**, 448–463.
Sakabe, N., Ikemizu, S., Sakabe, K., Higashi, T., Nagakawa, A. & Watanabe, N. (1995). *Weissenberg camera for macromolecules with imaging plate data collection at the Photon Factory – present status and future plan. Rev. Sci. Instrum.* **66**, 1276–1281.
Sayre, D. (2008). *Report on a project on three-dimensional imaging of the biological cell by single-particle X-ray diffraction*. *Acta Cryst.* A**64**, 33–35.
Schiltz, M. & Bricogne, G. (2009). *Instrument-independent specification of the diffraction geometry and polarization state of the incident X-ray beam*. *J. Appl. Cryst.* **42**, 101–108.
Schiltz, M., Kvick, Å., Svensson, O. S., Shepard, W., de La Fortelle, E., Prangé, T., Kahn, R., Bricogne, G. & Fourme, R. (1997). *Protein crystallography at ultra-short wavelengths: feasibility study of anomalous-dispersion experiments at the xenon K-edge. J. Synchrotron Rad.* **4**, 287–297.
Schwinger, J. (1949). *On the classical radiation of accelerated electrons. Phys. Rev.* **75**, 1912–1925.
Shapiro, D. A. (2008). *Report on a project on three-dimensional imaging of the biological cell by single-particle X-ray diffraction. Addendum*. *Acta Cryst.* A**64**, 36–37.
Snell, E. H., Weisgerber, S., Helliwell, J. R., Weckert, E., Hölzer, K. & Schroer, K. (1995). *Improvements in lysozyme protein crystal perfection through microgravity growth*. *Acta Cryst.* D**51**, 1099–1102.
Srajer, V., Teng, T. Y., Ursby, T., Pradervand, C., Ren, Z., Adachi, S., Schildkamp, W., Bourgeois, D., Wulff, M. & Moffat, K. (1996). *Photolysis of the carbon monoxide complex of myoglobin: nanosecond time-resolved crystallography. Science*, **274**, 1726–1729.
Stuhrmann, H. B. & Lehmann, M. S. (1994). *Anomalous dispersion of X-ray scattering from low Z elements*. In *Resonant Anomalous X-ray Scattering*, edited by G. Materlik, C. J. Sparks & K. Fischer, pp. 175–194. Berlin: Springer Verlag.
Sugahara, M., Asada, Y., Shimada, H., Taka, H. & Kunishima, N. (2009). *HATODAS II – heavy-atom database system with potentiality scoring*. *J. Appl. Cryst.* **42**, 540–544.
Tate, M. W., Eikenberry, E. F., Barna, S. L., Wall, M. E., Lowrance, J. L. & Gruner, S. M. (1995). *A large-format high-resolution area X-ray detector based on a fiber-optically bonded charge-coupled device (CCD). J. Appl. Cryst.* **28**, 196–205.
Templeton, D. H. & Templeton, L. K. (1985). *X-ray dichroism and anomalous scattering of potassium tetrachloroplatinate(II). Acta Cryst.* A**41**, 365–371.
Templeton, D. H., Templeton, L. K., Phillips, J. C. & Hodgson, K. O. (1980). *Anomalous scattering of X-rays by cesium and cobalt measured with synchrotron radiation. Acta Cryst.* A**36**, 436–442.
Templeton, L. K., Templeton, D. H., Phizackerley, R. P. & Hodgson, K. O. (1982). *$L_3$-edge anomalous scattering by gadolinium and samarium measured at high resolution with synchrotron radiation. Acta Cryst.* A**38**, 74–78.

Teplyakov, A., Oliva, G. & Polikarpov, I. (1998). *On the choice of an optimal wavelength in macromolecular crystallography. Acta Cryst.* D**54**, 610–614.

Tsukihara, T., Aoyama, H., Yamashita, E., Tomizaki, T., Yamaguchi, H., Shinzawa-Itoh, K., Nakashima, R., Yaono, R. & Yoshikawa, S. (1996). *The whole structure of the 13-subunit oxidized cytochrome c oxidase at 2.8 Å. Science*, **272**, 1136–1144.

Usha, R., Johnson, J. E., Moras, D., Thierry, J. C., Fourme, R. & Kahn, R. (1984). *Macromolecular crystallography with synchrotron radiation: collection and processing of data from crystals with a very large unit cell. J. Appl. Cryst.* **17**, 147–153.

Warren, J. E., Diakun, G., Bushnell-Wye, G., Fisher, S., Thalal, A., Helliwell, M. & Helliwell, J. R. (2008). *Science experiments via telepresence at a synchrotron radiation source facility*. *J. Synchrotron Rad.* **15**, 191–194.

Webb, N. G., Samson, S., Stroud, R. M., Gamble, R. C. & Baldeschwieler, J. D. (1977). *A focusing monochromator for small-angle diffraction studies with synchrotron radiation. J. Appl. Cryst.* **10**, 104–110.

Weckert, E. & Hümmer, K. (1997). *Multiple-beam X-ray diffraction for physical determination of reflection phases and its applications. Acta Cryst.* A**53**, 108–143.

Westbrook, E. M. & Naday, I. (1997). *Charge-coupled device-based area detectors. Methods Enzymol.* **276**, 244–268.

Wilson, K. S., Stura, E. A., Wild, D. L., Todd, R. J., Stuart, D. I., Babu, Y. S., Jenkins, J. A., Standing, T. S., Johnson, L. N., Fourme, R., Kahn, R., Gadet, A., Bartels, K. S. & Bartunik, H. D. (1983). *Macromolecular crystallography with synchrotron radiation. II. Results. J. Appl. Cryst.* **16**, 28–41.

Wimberley, B. T., Brodersen, D. E., Clemons, W. M., Morgan-Warren, R. J., Carter, A. P., Vonrhein, C., Hartsch, T. & Ramakrishnan, V. (2000). *Structure of the 30S ribosomal subunit*. *Nature (London)*, **407**, 327–339.

Winick, H. (1995). *The linac coherent light source (LCLS): a fourth-generation light source using the SLAC linac. J. Electron Spectrosc. Relat. Phenom.* **75**, 1–8.

Yano, J., Kern, J., Irrgang, K. D., Latimer, M. J., Bergmann, U., Glatzel, P., Pushkar, Y., Biesiadka, J., Loll, B., Sauer, K., Messinger, J., Zouni, A. & Yachandra, V. K. (2005). *X-ray damage to the Mn4Ca complex in single crystals of photosystem II: a case study for metalloprotein crystallography. Proc. Natl Acad. Sci. USA*, **102**, 12047–12052.

Yonath, A. (1992). *Approaching atomic resolution in crystallography of ribosomes. Annu. Rev. Biophys. Biomol. Struct.* **21**, 77–93.

Yonath, A., Harms, J., Hansen, H. A. S., Bashan, A., Schlünzen, F., Levin, I., Koelln, I., Tocilj, A., Agmon, I., Peretz, M., Bartels, H., Bennett, W. S., Krumbholz, S., Janell, D., Weinstein, S., Auerbach, T., Avila, H., Piolleti, M., Morlang, S. & Franceschi, F. (1998). *Crystallographic studies on the ribosome, a large macromolecular assembly exhibiting severe nonisomorphism, extreme beam sensitivity and no internal symmetry. Acta Cryst.* A**54**, 945–955.